https://doi.org/10.5194/egusphere-2026-2619
Preprint. Discussion started: 18 June 2026

Impact of satellite observations on assimilation inversion of high-resolution urban-scale carbon dioxide fluxes

Xingyu Yao[1,2], Ying Zhang[1,2,*], Xiaofan Li[1,2], Gerrit de Leeuw[1,3], Cheng Fan[1,2], Yuanxun Zhang[2], Zhanshan Wang[4], Yongjie Wei[4], Zhengqiang Li[1,2]

[1] State Environmental Protection Key Laboratory of Satellite Remote Sensing, Aerospace Information Research Institute, Chinese Academy of Sciences, Beijing 100101, China
[2] University of Chinese Academy of Sciences, Beijing 100049, China
[3] R&D Satellite Observations, Royal Netherlands Meteorological Institute (KNMI), 3730 AE De Bilt, The Netherlands
[4] State Key Laboratory of Environmental Criteria and Risk Assessment, Chinese Research Academy of Environmental Sciences, Beijing 10048, China

Correspondence to: Ying Zhang (zhang_ying@aircas.ac.cn)

Abstract. Cities are major sources of global carbon. Accurately quantifying urban-scale carbon dioxide (CO_2) fluxes is essential for supporting targeted emission reduction policies and effective monitoring. To address the limitations in the accuracy of current urban carbon emission estimates, we developed FEISSO, an urban-scale CO_2 flux inversion system that integrates a Lagrangian atmospheric transport model with a Bayesian assimilation framework. FEISSO was used to systematically explore the feasibility of retrieving high-resolution flux distributions from satellite-based XCO_2 observations. Sensitivity experiments were conducted in Weifang, Chengdu, and Xining (China) to identify key influencing factors in CO_2 flux inversion. Results show that the resolution of meteorological drivers substantially affects the accuracy of simulated transport trajectories, with higher resolution (0.25°) improving the spatial fidelity of flux retrieval. Sensitivity analysis indicates that the column-averaged CO_2 observation error and the total error for the inversion domain are the dominant factors affecting the total flux estimates, and they induce a "seesaw" effect in the spatial distribution of emissions. In contrast, prior flux error and spatial correlation length for land have limited influence on the total emissions but primarily affect the spatial pattern of weak emission regions and the smoothness of flux fields, respectively. Differences in topography and meteorological conditions across cities govern the temporal response of flux estimates to observations. With optimized parameter settings, the system successfully retrieved 10-days of total CO_2 emissions for Weifang, Chengdu, and Xining, showing overall consistency with EDGAR and local inventory data. The retrieved emissions correspond to 85.8%, 190.42%, and 86.4% of the EDGAR estimates for the three cities, respectively, while the relative differences from local inventories are 2.3% for Weifang and 10.9% for Xining. The results from this study demonstrate the applicability and scalability of the FEISSO system for urban CO_2 flux estimation. In this study, the frequency of urban-scale inversions was limited by the current orbital coverage of the OCO-2 satellite. With future improvements in satellite observation capabilities, particularly in spatial resolution and revisit frequency, FEISSO is expected to play a pivotal role in global urban carbon emission monitoring and in the evaluation of emission reduction policy.

https://doi.org/10.5194/egusphere-2026-2619
Preprint. Discussion started: 18 June 2026

1 Introduction

Carbon dioxide (CO_2) is a major greenhouse gas. The rapid increase concentration has substantially contributed to global warming and has triggered a cascade of climate related changes, with profound impacts on the Earth system(Kuo et al., 1990; Wang and Nemani, 2015; Friedlingstein et al., 2025). According to observations from the Global Monitoring Laboratory (GML), the global mean atmospheric CO_2 concentration increased from 280 ppm before the Industrial Revolution to 423.6 ppm in November 2024. The Intergovernmental Panel on Climate Change (IPCC) reported in the Climate Change 2023 AR6 Synthesis Report that the global mean surface temperature increased by 1.1 ˚C above pre industrial level, leading to sea level rise, more frequent extreme weather events, and ecosystem degradation, which together impose severe challenges and further destabilize the global climate system(Lee et al., 2023). In October 2018 the IPCC proposed the goal of limiting global warming to 1.5 ˚C as a critical threshold to safeguard the resilience of the Earth system(Masson-Delmotte et al., 2018). Large regional disparities in CO_2 emissions are evident across the globe. Although adaptation measures have alleviated part of the climate impacts, highly vulnerable populations and ecosystems still face substantial pressure and remain insufficiently protected from adverse effects due to climate change. Achieving global objectives for climate adaptation and mitigation requires long-term sustained and systematic efforts. Comprehensive and systematic characterization of the sources and sinks of atmospheric CO_2, together with quantitative assessment of the relative contributions from anthropogenic activities and natural processes to CO_2 emissions and uptake, is therefore of fundamental scientific importance for effective regulation of atmospheric CO_2 concentrations and for the mitigation of global climate change.

Although urban areas occupy only about 2% of the global land surface, they are home to more than 55% of the global population, and this proportion is projected to rise to 68% by 2050(Nations, 2019). Large populations, industries, and infrastructure are concentrated in urban areas, which leads to high levels of energy consumption. They function as major locations of anthropogenic activity, including fossil fuel combustion, industrial emission, deforestation, and land use change. These activities drive the continued increase in greenhouse gas concentrations and also weaken the capacity of ocean and terrestrial ecosystems to absorb these gases(Hebbert, 2012). Urban areas are estimated to account for between 67% and 72% of global greenhouse gas emissions, and they therefore play a central role in climate change mitigation(Shukla et al., 2022). The international community has strengthened its focus on mitigation efforts at the urban scale, and many initiatives for control and assessment have been implemented for cities(Bertelli et al., 2024). However, cities differ substantially in geography, climatic context, and resource endowment, which results in strong heterogeneity in energy structure and carbon emission characteristics. Differences in levels of socioeconomic development further lead to large contrasts in total emission, growth patterns, and mitigation pathways among cities. Fine scale estimation of CO_2 emissions across multiple urban scales and analysis of their structural and spatial distribution characteristics are essential for the formulation of differentiated and operational mitigation policies. These efforts facilitate the identification of urban carbon emission hotspots and enhance mitigation efficiency while also providing important scientific support for national and global greenhouse gas reduction strategies.

https://doi.org/10.5194/egusphere-2026-2619
Preprint. Discussion started: 18 June 2026

Spatiotemporal information on CO_2 emissions is primarily derived through two approaches, namely the bottom up method and the top down method. The bottom up method mainly relies on survey based statistics and simulates CO_2 emission through empirical models(Detling et al., 1978; Beer et al., 2010) or process based models(Thornton et al., 2002; Sato et al., 2007; Stagakis et al., 2023; Zhang et al., 2026). However, this method is limited by low temporal resolution and by substantial uncertainties introduced through anthropogenic modeling assumptions(Zhang et al., 2025; Song et al., 2024). The top down method constrains prior emission inventories using observational data and mainly depends on atmospheric measurements, data assimilation techniques, and atmospheric transport models. In recent years, advances in observational technology, including the wider deployment of ground based observation networks and major progress in satellite remote sensing, have markedly strengthened the role of the top down method in the estimation of carbon sources. At the global scale, projects such as GLOBALVIEW Plus and the Total Carbon Column Observing Network have provided extensive ground based measurement records. Meanwhile, the launch of a series of satellite sensors such as SCIAMACHY, GOSAT, TanSat, GOSAT 2, the Orbiting Carbon Observatory 2 mission, and the Orbiting Carbon Observatory 3 mission has greatly improved the spatiotemporal resolution and accuracy of column averaged CO_2 observations. For example, relative to the spatial resolution of approximately 30 km × 60 km for SCIAMACHY, the Orbiting Carbon Observatory missions achieve footprints on the order of about 1.29 km × 2.25 km, and the uncertainty of column averaged CO_2 retrievals has been reduced from about 14 ppm to less than 1 ppm(Liu et al., 2022; O'dell et al., 2018). At the urban scale, ground based stations can provide highly accurate observations, but their deployment is constrained by site availability, and the high cost of construction and maintenance limits large scale implementation. Moreover, only a limited number of cities have established dense urban CO_2 monitoring networks(Han et al., 2024; Aigner et al., 2026). In contrast, satellite remote sensing offers advantages in objectivity, continuity, stability, wide spatial coverage, and repeat observation capability. As a result, satellite observations have become an essential means for achieving high accuracy and high resolution estimation of CO_2 emissions at the urban scale(Hu et al., 2024; Zhao et al., 2026). Atmospheric CO_2 flux data assimilation and inversion have achieved substantial progress in recent years, and multiple inversion systems based on different modeling frameworks have been developed(Chevallier et al., 2019; Su et al., 2024). These systems generally ingest ground based observations or satellite derived column averaged CO_2 products as input and aim to estimate and analyze the spatial distribution of CO_2 sources and sinks at global or national scales. However, inversion of CO_2 fluxes at the urban scale remains insufficiently explored, and methodological development and system construction are still at an early stage. Existing studies at the urban scale mainly rely on tall tower measurements(Lauvaux et al., 2016; Kunz et al., 2026) or ground based observation networks(Kunik et al., 2019; Lian et al., 2024; Aigner et al., 2026). The high logistical complexity together with the cost of deployment and maintenance constrains the scalability of this approach. Data assimilation inversions that use satellite based column averaged CO_2 observations remain concentrated in Observing System Simulation Experiments (OSSEs)(Ye et al., 2020), and their effectiveness for real world estimation of urban CO_2 fluxes has not yet been comprehensively verified. Advancing research on urban scale inversion of CO_2 fluxes therefore has important theoretical value and practical relevance.

https://doi.org/10.5194/egusphere-2026-2619
Preprint. Discussion started: 18 June 2026

Most mainstream flux inversion systems employ Eulerian atmospheric transport models to simulate the transport and dispersion of CO_2 in the atmosphere. Representative systems include the CarbonTracker system of NOAA(Peters et al., 2007; Jacobson et al., 2023), the Copernicus Atmosphere Monitoring Service of ECMWF(Chevallier et al., 2005; Remaud et al., 2018), the Jena CarboScope system of the Max Planck Institute for Biogeochemistry(Rödenbeck et al., 2014; Rödenbeck et al., 2022), the GCAS v2 system developed at Nanjing University(Jiang et al., 2021), and the GONGGA system developed by the Institute of Tibetan Plateau Research of the Chinese Academy of Sciences(Jin et al., 2023). Eulerian transport models provide mature and robust performance at large spatial scales, yet they face limitations in applications at the urban scale, particularly in representing fine scale transport structures, adapting to complex terrain, and managing computational cost. Lagrangian transport models simulate the trajectories of air parcels or particles and provide higher spatial resolution together with stronger adaptability to sparse observations and complex terrain, which makes them advantageous for urban scale inversion of CO_2 fluxes.

With respect to data assimilation and inversion algorithms, different systems adopt different methodological frameworks. Systems such as CarbonTracker(Peters et al., 2007), COLA(Liu et al., 2022), and GCAS v2(Jiang et al., 2021) mainly employ the Ensemble Kalman Filter for flux estimation, whereas systems such as CAMS(Friedlingstein et al., 2025), THU(Friedlingstein et al., 2025) and GONGGA(Jin et al., 2023) adopt a four dimensional variational assimilation framework. Although these algorithms have been extensively applied at the mesoscale and at the global scale, the Bayesian inversion framework provides greater flexibility and adaptability at the urban scale, where observational heterogeneity, large uncertainties, and nonlinear behavior are more pronounced. The Bayesian framework supports explicit quantification of inversion uncertainty and can effectively address nonlinear processes, and it has therefore been increasingly applied in recent urban scale inversion studies with encouraging results(Kunik et al., 2019; Nickless et al., 2019; Roten et al., 2023; Hamilton et al., 2024). In summary, inversion of CO_2 fluxes at the urban scale faces concurrent challenges associated with high resolution simulation requirements and sparse observational coverage. Inversion systems that combine Lagrangian atmospheric transport models with Bayesian inversion frameworks exhibit higher adaptability and improved estimation accuracy and are well suited for refined assessment of urban carbon emissions.

In this study we developed an urban scale carbon flux inversion system named the FEISSO (Flux and Emission Inversion System for Satellite Observation) assimilation system, which is based on a Lagrangian atmospheric transport model and employs a data assimilation framework based on Bayesian theory. The system uses satellite-retrieved XCO_2, defined as the column-averaged dry-air mole fraction of atmospheric CO_2, to investigate the feasibility of deriving high-resolution urban-scale CO_2 flux distributions from satellite observations. To evaluate the sensitivity of inversion results to key parameters we selected three cities, Weifang, Chengdu, and Xining, which differ in geographic setting and in level of economic development, as case studies for systematic sensitivity experiments. The objectives of this study are (1) to identify the major factors that control the accuracy and stability of urban scale inversion of CO_2 fluxes, and (2) to extract both common patterns and region specific characteristics. To achieves these objectives, the influence of satellite observation accuracy, prior flux uncertainty,

https://doi.org/10.5194/egusphere-2026-2619
Preprint. Discussion started: 18 June 2026

and the spatial resolution of meteorological fields on the inversion results are examined. This research provides methodological guidance and recommendations for parameter selection for high accuracy and high resolution estimation of CO_2 emissions at the urban scale and has both scientific significance and practical application value. The structural design and theoretical basis of the FEISSO system are presented in Section 2. Results are presented in Section 3 and discussed in Section 4. Conclusions are presented in Section 5.

2 Method and Data

2.1 FEISSO-Carbon

We developed a greenhouse gas flux assimilation system named FEISSO-Carbon (Flux and Emission Inversion System for Satellite Observation). The system ingests satellite-based observations of column-averaged mixing ratios and combines a Lagrangian atmospheric transport model with a Bayesian inversion framework, to assimilate greenhouse gas fluxes at multiple scales and resolutions, including high-resolution urban-scale, medium-resolution national-scale, and low-resolution global-scale inversions. In this study, we primarily focus on urban-scale flux inversion. FEISSO-Carbon employs a dual-nested grid strategy, decomposing the contributions of column-averaged mixing ratios into regional, global, and background components, thereby enabling a more refined characterization of emission source structures and improving the accuracy of regional contribution estimates.

The FEISSO-Carbon system comprises five core modules, with its overall architecture illustrated in Fig. 1. The system takes satellite-derived column-averaged CO_2 mixing ratios as input and, driven by meteorological fields, applies the Lagrangian particle dispersion model FLEXPART(Stohl et al., 1998; Pisso et al., 2019) to perform backward trajectory simulations, generating layered source-receptor relationships (SRRs). These layered SRRs are further refined through a convolution process that incorporates prior mixing ratios information from satellite products, kernel functions, and pressure weighting functions, yielding improved column-averaged SRRs. Multi-source emission inventories, after prior flux optimization, provide high-resolution spatial distributions of emissions as prior input. These are combined with the column-averaged SRRs through multiplication to estimate the contributions of surface emissions to the global and regional observations. In parallel, a calibrated background field is introduced to estimate the contribution of background mixing ratios, which is then combined with the surface contributions to obtain the forward-simulated mixing ratios. The simulated mixing ratios are compared with satellite observations, and the Bayesian assimilation framework FLEXINVERT+(Thompson and Stohl, 2014) is employed to retrieve the high-resolution spatial and temporal distribution of greenhouse gas emissions at the urban scale.

https://doi.org/10.5194/egusphere-2026-2619
Preprint. Discussion started: 18 June 2026

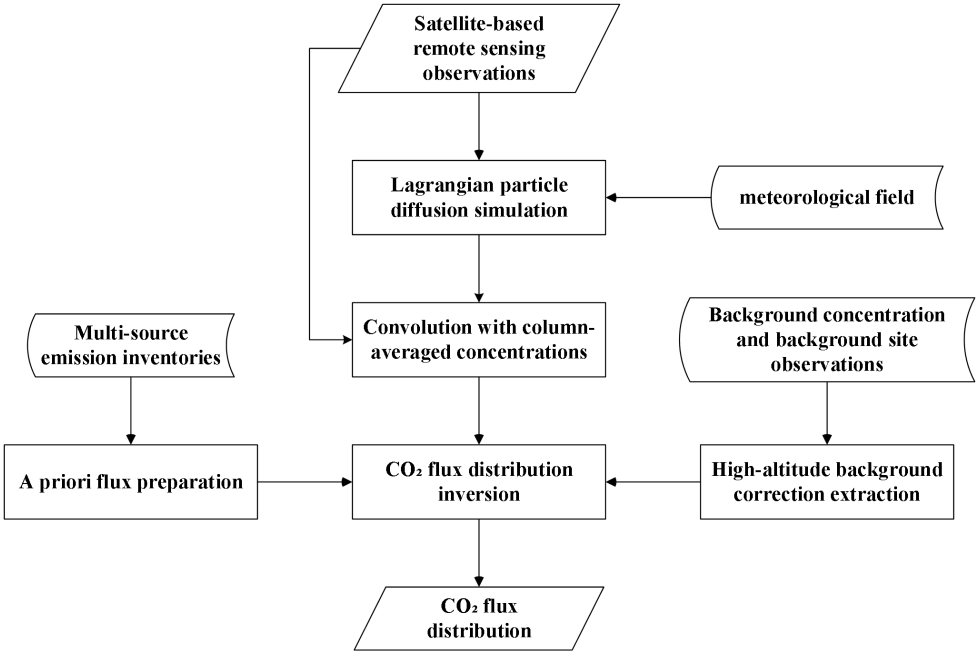

Figure 1: Schematic Structure of the FEISSO-Carbon Inversion System

2.1.1 FLEXPART

FEISSO-Carbon utilizes FLEXPART to perform backward trajectory simulations of atmospheric CO_2 particles, thereby quantifying the contribution of surface emissions to the observed CO_2 mixing ratios at receptor locations. FLEXPART, a Lagrangian particle dispersion model, is widely used to simulate the transport and mixing of trace gases in the atmosphere. FLEXPART can simulate the trajectories of particles released from point, line, area, or volumetric sources, incorporating atmospheric transport, diffusion, dry and wet deposition, radioactive decay, and first-order chemical reactions(Stohl, 1998; Stohl et al., 2005). These simulations yield temporally and spatially resolved SRRs (Thomson, 1987), which characterize the contributions of surface emissions from different regions to receptor-site CO_2 mixing ratios.

In this study, we employed version 10.4 of FLEXPART (https://www.flexpart.eu/) to release particles at each receptor location and track them backward in time to compute the corresponding SRRs(Pisso et al., 2019). Previous studies have commonly used ECMWF reanalysis datasets with spatial resolutions of 1°×1° or 0.5°×0.5° to drive FLEXPART(Thompson and Stohl, 2014; Thompson et al., 2025). However, our findings indicate that for urban-scale CO_2 source attribution, the spatial resolution of meteorological fields plays a critical role in accurately resolving the transport pathways of atmospheric CO_2 (see Section 3.1 for details). Accordingly, we used the NCEP Final (FNL) operational global analysis data with a spatial resolution of 0.25°×0.25° to drive the FLEXPART model, enabling global-scale backward trajectory simulations of CO_2 transport at 0.25°×0.25° resolution. Within the targeted study domains, backward trajectory simulations were further refined to a spatial resolution of 0.01°×0.01°, allowing for high-resolution attribution of CO_2 transport pathways at the urban scale.

https://doi.org/10.5194/egusphere-2026-2619
Preprint. Discussion started: 18 June 2026

2.1.2 FLEXINVERT+

FEISSO-Carbon is built upon the Bayesian inversion framework FLEXINVERT+ and employs a two-level nested configuration to assimilate urban-scale CO_2 fluxes, yielding high-resolution spatial estimates of CO_2 emissions. FLEXINVERT+ models atmospheric transport using a linear forward operator **H**, and derives the optimal solution using Bayes' theorem. The most probable solution x minimizes the mismatch between observed and modeled mixing ratios, while incorporating prior state estimates x_b and their associated uncertainties(Tarantola, 2005). Assuming Gaussian-distributed uncertainties, the cost function **J(x)** is formulated as:

$$J(\mathbf{x}) = \frac{1}{2}(x - x_b)^T \mathbf{B}^{-1}(x - x_b) + \frac{1}{2}\left(\mathbf{H}x - y^{\text{obs}}\right)^T \mathbf{R}^{-1}\left(\mathbf{H}x - y^{\text{obs}}\right) \quad (1)$$

where $\mathbf{B}_{(N\times N)}$ is the prior flux error covariance matrix, $\mathbf{R}_{(M\times M)}$ is the observation error covariance matrix, and y^{obs} is the vector of observed mixing ratios.

Solving for the minimum of the cost function J yields the posterior flux estimate. Several methods exist to minimize Eq.(1); in this study, we employ a first-order derivative approach, which leads to the rearranged form:

$$x = x_b + \mathbf{B}\mathbf{H}^T\left(\mathbf{H}\mathbf{B}\mathbf{H}^T + \mathbf{R}\right)^{-1}\left(y^{\text{obs}} - \mathbf{H}\mathbf{x}_b\right) \quad (2)$$

Here, the matrix $(\mathbf{HBH}^T + \mathbf{R})$ of size $M \times M$ is inverted via Cholesky decomposition to improve computational efficiency. The corresponding posterior error covariance matrix A is given by the second derivative (Hessian) of the cost function:

$$A = \left(J''\right)^{-1} = B - BH^T\left(HBH^T + R\right)^{-1}HB \quad (3)$$

To address computational efficiency issues caused by the high spatial resolution, we apply a truncation method to the eigenvalue decomposition during inversion, which significantly accelerates the assimilation process without compromising the accuracy of the urban-scale CO_2 flux estimates.

2.1.3 Layer-by-Layer convolution improvement for atmospheric columns

Current Lagrangian-based atmospheric inversion methods, such as FLEXPART-FLEXINVERT, are primarily designed for assimilating ground-based observations. These models simulate CO_2 mixing ratios corresponding to specific vertical layers in the atmosphere. In contrast, satellite-based column-averaged CO_2 mixing ratios are derived from the convolution of mixing ratios across multiple atmospheric layers. Therefore, it is necessary to convolve the model-simulated mixing ratios from different vertical layers to ensure consistency with satellite observations. In this study, we convolve the model-simulated mixing ratios from different vertical layers using the same algorithm employed by satellite retrievals, thereby generating forward-simulated values consistent with satellite column-averaged mixing ratios.

According to (Connor et al., 2008), the OCO-retrieved profile-weighted CO_2 mixing ratio (XCO_2) and its total uncertainty σ^2_{total} are insufficient on their own for accurately inferring surface fluxes via inversion or data assimilation. Additional

https://doi.org/10.5194/egusphere-2026-2619
Preprint. Discussion started: 18 June 2026

information, including the OCO measurements under a given CO_2 vertical profile, atmospheric state, and surface conditions, must be simulated. The OCO-retrieved XCO_2 can be expressed as:

$$\boldsymbol{X}_{CO2} = \boldsymbol{X}^{a}_{CO2} + \sum\nolimits_{j} \boldsymbol{h}_j \boldsymbol{a}_{CO2,j} \left(\boldsymbol{x} - \boldsymbol{x}_a \right)_j \tag{4}$$

where $\boldsymbol{X}^{a}_{CO2}$ denotes the prior XCO_2 value, $\boldsymbol{h}$ represents the pressure weighting function for each atmospheric layer, and $\boldsymbol{a}$ is the averaging kernel associated with each layer during the convolution to the column-mean value. Similarly, the simulated column-averaged CO_2 concentration can be expressed as the convolution of layer-specific simulated mixing ratios:

$$\boldsymbol{X}^{m}_{CO2} = \boldsymbol{X}^{a}_{CO2} + \sum\nolimits_{j} \boldsymbol{h}_j \boldsymbol{a}_{CO2,j} \left(\boldsymbol{x}_{\boldsymbol{m}} - \boldsymbol{x}_a \right)_j \tag{5}$$

By applying the forward model to simulate CO_2 mixing ratios at each contributing atmospheric layer, and substituting Equation (5) into the FLEXINVERT+ framework, we compute the modeled satellite-observed column-averaged CO_2 concentration via convolution, as expressed in Equation(6).

$$\begin{aligned} XCO2_2^{\mathrm{mod}} &= (XCO2_2^{a} - \sum a_j \cdot \mathrm{h}_j \cdot y^{a}) \\ &+ f^{nest} \cdot \sum a_j \cdot \mathrm{h}_j \cdot H^{nest} + f^{out} \cdot \sum a_j \cdot \mathrm{h}_j \cdot H^{out} + y^{bg} \cdot \sum a_j \cdot \mathrm{h}_j \cdot H^{bg} \end{aligned} \tag{6}$$

In the column convolution process, all prior mixing ratios, pressure weighting functions, and averaging kernels used in this study are directly derived from the satellite XCO_2 product. This satellite-based parameter configuration avoids uncertainties arising from additional assumptions and ensures the physical consistency and reliability of the column convolution results. Our algorithm is consistent with the normalization approach for column-averaged CO_2 mixing ratios described by Thompson et al. (2025) (Thompson et al., 2025), while offering greater flexibility in its application. Thompson et al. (2025) directly modified the FLEXPART model to enable stratified simulations of CO_2 particle trajectories during atmospheric transport, yielding normalized SRRs. Since SRRs quantify the contribution of emission sources to the CO_2 mole fraction at a specific receptor location, they are inherently independent of the vertical stratification details in atmospheric transport. Consequently, our atmospheric column convolution framework operates independently of any particular atmospheric dispersion model and supports both normalization and vertical resolution adjustments. It can be readily adapted to various satellite platforms, observational strategies, and product characteristics, offering broad applicability and considerable potential across a wide range of scientific applications.

2.1.4 Correction of background CO_2 concentration fields

Since Lagrangian atmospheric transport models can generally trace air parcels backward in time only for several days to several weeks(Thompson and Stohl, 2014), it is necessary to represent the CO_2 concentration at the termination point of the backward trajectories, which is treated as the background mixing ratio. The background mixing ratio is defined as a long term and relatively stable atmospheric CO_2 concentration that is not influenced by local surface emissions. To improve the accuracy of this background field, a series of corrections are applied to the simulated mixing ratios.

https://doi.org/10.5194/egusphere-2026-2619
Preprint. Discussion started: 18 June 2026

First, the GEOS Chem model is used to simulate the three dimensional spatiotemporal distribution of atmospheric CO_2 mixing ratios over an extended period. The simulated mixing ratios are then calibrated through vertical profile fitting based on 84 historical AirCore aircraft observations obtained during the period from 2012 to 2021 and provided by NOAA's Global Monitoring Laboratory (https://gml.noaa.gov/ccgg/aircore/). This procedure yields background values of CO_2 that more closely approximate actual atmospheric conditions. In order to remove the influence of surface emissions on the background field, CO_2 mixing ratios are extracted at three upper atmospheric pressure levels, namely 510.475 hectopascal, 139.115 hectopascal, and 48.282 hectopascal, and these values are used as the background mixing ratios in the regional assimilation and inversion of CO_2 fluxes.

2.1.5 Prior Fluxes

For the prior fluxes of CO_2, we consider three components: anthropogenic emissions, terrestrial net ecosystem exchange (NEE), and oceanic fluxes. As FEISSO-Carbon estimates CO_2 fluxes for the target region using a two-level nested framework, prior fluxes are specified at both coarse-resolution global scales and high-resolution urban scales.

For anthropogenic emissions, at the global scale, we interpolate the EDGAR 2023 (Crippa et al., 2024)CO_2 emission inventory from its original $0.1^\circ \times 0.1^\circ$ resolution to $1^\circ \times 1^\circ$ and $0.25^\circ \times 0.25^\circ$, to assess the impact of different meteorological data resolutions and prior inventories on regional high-resolution CO_2 flux inversions. At the regional scale, we combine the finer spatial distribution of the ODIAC inventory(Oda et al., 2018) with the more accurate total emissions estimates from EDGAR to derive CO_2 fluxes at $0.01^\circ \times 0.01^\circ$ resolution within the target area.

For terrestrial net ecosystem exchange, we interpolate the CT2019B product to $1^\circ \times 1^\circ$ and $0.25^\circ \times 0.25^\circ$ resolution at the global scale. Within the nested domain, we simulate NEE at $0.01^\circ \times 0.01^\circ$ resolution using the WRF-GHG (Weather Research and Forecasting model with Greenhouse Gases module) to achieve finer and more accurate representation of land-atmosphere CO_2 exchange at the urban scale. WRF-GHG is a mesoscale atmospheric-greenhouse gas coupled model that incorporates the Vegetation Photosynthesis and Respiration Model (VPRM), enabling high-resolution simulation of regional carbon fluxes and the spatiotemporal distribution of atmospheric CO_2 mixing ratios. The enhanced vegetation index (EVI) and land surface water index (LSWI) are derived at 1 km resolution utilizing MODIS Level 3 8-day composite surface reflectance products at 500 m resolution, and interpolate them spatiotemporally. The WRF model provides spatially resolved hourly meteorological fields, soil conditions, and photosynthetically active radiation (PAR), which are used to drive the VPRM to dynamically simulate NEE at $0.01^\circ \times 0.01^\circ$ resolution.

For oceanic fluxes, we interpolate the global CO2v2014 product to resolutions of $1^\circ \times 1^\circ$ and $0.25^\circ \times 0.25^\circ$ at the global scale. If the study area includes coastal cities, oceanic fluxes are further interpolated to 0.01° resolution within the nested domain; otherwise, they are omitted.

https://doi.org/10.5194/egusphere-2026-2619
Preprint. Discussion started: 18 June 2026

2.1 Study area and satellite observations

2.2.1 Study regions

To comprehensively assess the performance of the FEISSO-Carbon assimilation system in estimating high-resolution urban-scale CO_2 emission fluxes, we selected three cities in China that represent diverse geographic locations and levels of economic development: Weifang in Shandong Province, Chengdu in Sichuan Province, and Xining in Qinghai Province. The geographic locations and topographic characteristics of these cities are shown in Fig. 2.

From an economic perspective, Chengdu, as the economic hub of southwestern China, reported a gross domestic product (GDP) of 2.3 trillion CNY in 2024, ranking eighth among Chinese cities. The EDGAR database shows that the annual CO_2 emission in Chengdu was 131.48×10^6 t in 2023. Weifang is located in the economically developed eastern coastal region and benefits from favorable geographic and industrial conditions. Its economic output is slightly lower than that of Chengdu, with a GDP of approximately 820.32 billion CNY in 2024. The annual CO_2 emission in 2023 was 42.238×10^6 t, as reported by EDGAR. Xining is located on the Qinghai-Tibet Plateau, within China's second topographic step. Due to its geographic constraints and limited resource endowment, its economic development lags behind that of the other two cities. Its GDP in 2024 was approximately 180 billion CNY. Xining's annual CO_2 emission in 2023 reported by EDGAR was 24.149×10^6 t(Crippa et al., 2024).

In terms of topography, Weifang is situated on the flat eastern coastal plain, which is favorable for transportation and industrial development. Chengdu lies in the western part of the Sichuan Basin, which is enclosed and characterized by terrain that is higher in the west and lower in the east. The basin effect is pronounced, making it less favorable for the dispersion of air pollutants and ventilation out of the basin. Xining is located in a complex terrain zone of interlaced plateaus, mountains, and river valleys. The region exhibits substantial topographic variation and limited air circulation, leading to the frequent accumulation of pollutants, particularly during the winter heating season. The three study areas exhibit contrasting geographic settings, with Weifang, Chengdu, and Xining, thereby providing representative cases for evaluating urban-scale CO_2 flux inversions under different environmental and development conditions.

https://doi.org/10.5194/egusphere-2026-2619
Preprint. Discussion started: 18 June 2026

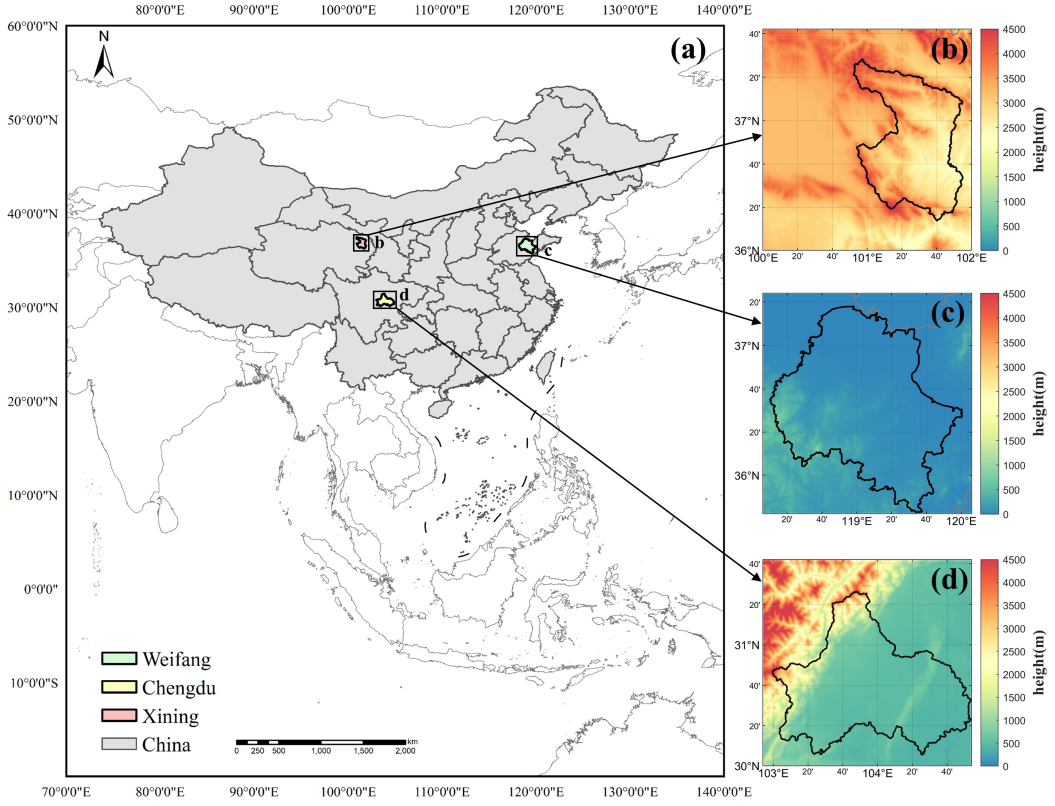

Figure 2: Geographic Location and Elevation Maps of China (a), Xining (b), Weifang (c), and Chengdu (d)

2.2.2 OCO-2 XCO_2 observational data

In this study, we utilize XCO_2 observations from the Orbiting Carbon Observatory-2 (OCO-2) as the observational input for the FEISSO-Carbon assimilation system. Launched in July 2014, OCO-2 operates in a sun-synchronous orbit at an altitude of 705 km and an inclination of 98.2°, with an orbital period of 98.82 minutes and a 16-day revisit cycle. The local overpass time is approximately 13:36. OCO-2 employs three observation modes: nadir, glint, and target. With a spatial resolution of 2.25 km × 1.29 km, OCO-2 meets the requirements for estimating high-resolution CO_2 emission fluxes at the urban scale using the FEISSO-Carbon system.

Among the multiple product versions available for OCO-2 XCO_2, we adopt the version 11.1 column-averaged CO_2 product in this study. As noted by Crisp et al. (2021), the single-retrieval uncertainty of XCO_2 in version 11.1 is less than 0.5 ppm, with total errors generally below 1.0 ppm. Compared to earlier versions, v11.1 introduces significant improvements in aerosol correction, atmospheric scattering modeling, and orbital calibration, resulting in reduced systematic and random errors(Crisp et al., 2021). Compared with other satellite products such as GOSAT and TanSat, OCO-2 v11.1 offers higher spatial resolution,

https://doi.org/10.5194/egusphere-2026-2619
Preprint. Discussion started: 18 June 2026

lower uncertainty, and a richer set of ancillary retrieval parameters, making it more suitable and advantageous for urban-scale carbon emission studies. The orbit tracks corresponding to the study periods and regions for each of the three cities are listed in Table 1. As our study focuses on a 1 km × 1 km grid resolution, which does not align precisely with the OCO-2 observation footprint, we resample the OCO-2 product. A "super observation" is defined as the median of all observations within one standard deviation in each 1 km × 1 km grid cell. Consequently, the numbers of super observations during the study periods are 829 for Weifang (35.7-37.4°N, 118.1-120.1°E), 311 for Chengdu (30.05-31.26°N, 102.54-104.53°E), and 676 for Xining (36.27-36.56°N, 101.18-101.52°E), respectively.

Table 1 Table of OCO-2 Data Used in This Study

Num	Study Area	Study Period	OCO-2 Track Number	Number of Super Observations
1	Weifang	2023.01.27-2023.02.05	45594, 45623, 45725	829
2	Chengdu	2023.03.06-2023.03.15	46250	311
3	Xining	2023.11.25-2023.12.04	50007, 50080, 50109	676

2.3 Experimental design

To evaluate the impacts of meteorological field resolution and system parameter sensitivity on the spatial distribution and total amount of CO_2 emissions, we designed a series of sensitivity experiments. In terms of prior flux specification, FEISSO employs a two-way nesting strategy to efficiently estimate high-resolution urban CO2 fluxes. We first evaluated the influence of meteorological fields from the outer domain by comparing inversion results driven by resolutions of 1° × 1° and 0.25° × 0.25°. The corresponding experiments and their impacts on inversion performance are discussed in Sect. 3.

For the nested domain covering the study area, a finer spatial resolution of 0.01° × 0.01° was adopted. EDGAR provides widely accepted estimates of total anthropogenic CO_2 emissions(Ahn et al., 2023), whereas ODIAC provides finer spatial emission patterns. Therefore, the total CO_2 emissions from EDGAR were redistributed according to the spatial distribution of ODIAC to construct the prior fluxes in the nested domain. This approach provides prior fluxes with both high spatial resolution (0.01°) and improved spatial representativeness.

In the system parameter sensitivity analysis, we focused on five key parameters: observation error (ObsErr), total flux error for the inversion domain (GlobErr), prior flux error (FlxErr), spatial correlation length over land (SigLand), and temporal correlation length (SigTime). These parameters characterize the influences of observational precision, overall regional emission uncertainty, prior flux uncertainty, the spatial extent of emission impacts on receptor concentrations, and the timescale of emission impacts on receptor concentrations, respectively. Each parameter was analyzed individually by varying its value while holding the others constant to assess its influence on regional CO_2 flux inversion. The tested ranges included observation errors of column-averaged CO_2 (0.5-5 ppm), domain-wide total CO_2 flux uncertainties (1%-25% of annual city-level CO_2 emissions), prior flux uncertainties (1%-30%), land spatial correlation lengths (10-50 km), and temporal correlation lengths (1-21 days). The sensitivity experiment design is summarized in Table 2. During the sensitivity tests, the default parameter values were set as follows: ObsErr was set to 1 ppm; GlobErr was calculated as twice the emission growth rate plus

https://doi.org/10.5194/egusphere-2026-2619
Preprint. Discussion started: 18 June 2026

the known difference between the prior inventory and local statistical data; FlxErr was set to 10%; SigLand to 25 km; and SigTime to 7 days.

Table 2 Experimental Design Table for System Parameter Sensitivity Analysis

Spatial resolution of meteorological fields		1°×1°	0.25°×0.25°					
			Exp 1	Exp 2	Exp 3	Exp 4	Exp 5	Exp 6
ObsErr (ppm)		1.0	0.5	0.7	1.0	2.0	3.0	5.0
GlobErr(% of a priori annual total emissions)	Weifang	15%	1%	5%	10%	15%	20%	25%
	Chengdu	15%	1%	5%	10%	15%	20%	25%
	Xining	10%	1%	5%	10%	15%	20%	25%
FlxErr		10%	1%	5%	10%	15%	20%	30%
SigLand(km)		25.0	10.0	15.0	20.0	25.0	30.0	50.0
SigTime(day)		7	1	3	7	10	14	21

To assess the influence of wind field resolution on regional CO_2 flux inversions, we conducted backward simulations using two versions of NCEP Final Operational Global Analysis (FNL) data at resolutions of 1° × 1° and 0.25° × 0.25°, to establish the relationship between satellite observations and surface fluxes. By comparing the inversion results derived from different-resolution meteorological inputs, we clarified the role of wind field resolution in the FEISSO-Carbon assimilation system and its impact on regional CO_2 flux estimates.

3 Results

3.1 Sensitivity to meteorological field spatial resolution

In this study, an atmospheric transport model is used to trace the observed variations in CO_2 mixing ratios backward in time, in order to adjust surface-atmosphere CO_2 fluxes. As such, accurately simulating atmospheric transport is essential for reliable surface flux quantification. The FLEXPART model used in this study is driven by meteorological reanalysis data and calculates the relationship between observation points (receptors) and surface fluxes (sources/sinks) via the source-receptor relationship (SSR). Thus, the accuracy of the meteorological fields driving the transport model is critically important, especially since the horizontal spatial resolution of meteorological inputs strongly influences the fidelity of local wind field simulations(Giovannini et al., 2014; Varghese et al., 2011). We conducted global simulations of column-averaged CO_2 mixing ratios using meteorological fields at 0.25° and 1° resolution, and compared them against satellite observations to evaluate how meteorological resolution influences the accuracy of simulated CO_2 columns.

Figure 3 presents a comparison between simulated and observed column averaged CO_2 mixing ratios for the three study cities, including the mean absolute error and the statistical distribution of simulation errors. The results in Fig. 3a show that simulations driven by meteorological fields with a spatial resolution of 0.25° produce mixing ratios that are closer to observations, with mean absolute errors of 0.69 ppm for Weifang and 1.09 ppm for Chengdu, representing 2.7 fold and 3.6 fold improvements relative to simulations with a resolution of 1°. In Chengdu, the mean absolute error with a 1° resolution can reach 3.89 ppm. Given the complex topography in this region and the large elevation decrease from the northwest to the

https://doi.org/10.5194/egusphere-2026-2619
Preprint. Discussion started: 18 June 2026

Sichuan Basin, the higher resolution meteorological field improves the representation of local transport processes and enhances the simulation of column averaged CO_2.

Figure 3b shows the statistical characteristics of the simulation errors. For the 0.25° simulations, the median bias fluctuates around zero, while the 1° simulations exhibit larger systematic bias. Consistent with the mean absolute error results, Chengdu shows the largest overall error range, with a wider spread between minimum and maximum errors than the other two cities. The 0.25° simulations reduce the systematic overestimation in Chengdu and produce a more concentrated error distribution with fewer extreme deviations. In Weifang, the median error also improves markedly at 0.25° resolution, and the interquartile range decreases from 0.81 ppm to 3.12 ppm to a range from -0.88 ppm to 0.05 ppm, which indicates that half of the errors are smaller than 1 ppm and the overall simulation error is constrained within 5 ppm. In Xining, the deviation at 1° resolution is already small, with a mean absolute error of 1.00 ppm, and the improvement at 0.25° resolution is therefore limited.

Overall, meteorological fields with a spatial resolution of 0.25° improve the representation of local transport features in urban CO_2 simulations and enhance the reliability of the inversion results, and this resolution is therefore adopted as the standard configuration in the subsequent sensitivity experiments.

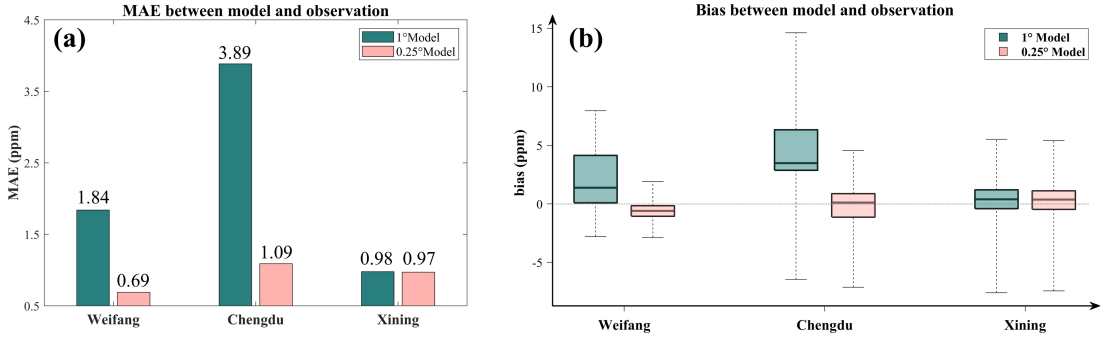

Figure 3: The effect of atmospheric transport model resolution on simulated XCO_2 fields. (a) absolute mean deviation between the simulated XCO_2 and satellite observations for the three cities at 1° and 0.25° resolution; (b) distribution of deviations between the simulated XCO_2 and satellite observations for the three cities at 1° and 0.25° resolution. The box represents the upper and lower quartiles of the deviations, the center line indicates the median, and the whiskers indicate the maximum/minimum values of the deviations

3.2 Total emission adjustment effects of model parameters

A 10-day CO_2 emission inversion sensitivity experiment was conducted for Weifang, Chengdu, and Xining, during which total CO_2 emissions were calculated using different combinations of parameter settings for each city, as described in Section 2.3. The sensitivity of the 10-day total CO_2 emissions to individual parameters is illustrated in Fig. 4, for the three cities. For each parameter, the x-axis corresponds to Exp1 to Exp6 from left to right.

https://doi.org/10.5194/egusphere-2026-2619
Preprint. Discussion started: 18 June 2026

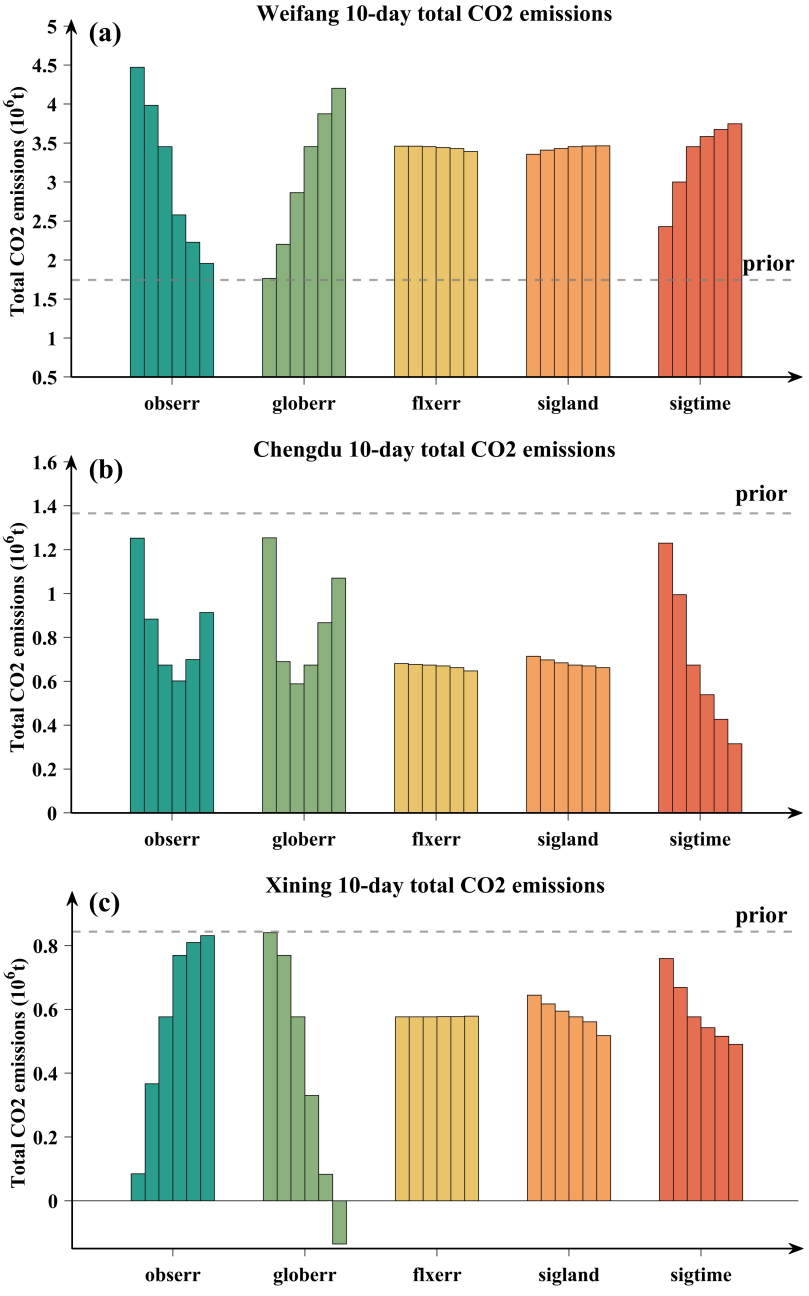

385 **Figure 4: Sensitivity of 10-day total CO_2 Emissions to the settings of model parameters for (a) Weifang; (b) Chengdu; (c) Xining . All experiments were made using meteorological fields with a spatial resolution of 0.25°. The values of the parameters are provided in Table 2, e.g. ObsErr varies from 0.5 to 5.0 (left to right), etc.**

Overall, ObsErr and GlobErr exert the most pronounced influence on regional CO_2 emission estimates, followed by the SigTime. In contrast, changes in FlxErr and SigLand have small effects relative to the other three parameters, resulting in
390 limited adjustments to total emissions.

https://doi.org/10.5194/egusphere-2026-2619
Preprint. Discussion started: 18 June 2026

In Weifang and Xining, the variation of CO_2 emissions with increasing ObsErr and GlobErr shows opposite trends in the two cities. As ObsErr decreases and GlobErr increases, the ten day cumulative CO_2 emissions in Weifang and Xining gradually deviate from the prior inventory estimates. This pattern indicates that with higher observational accuracy and weaker total flux constraints, the inversion system is able to adjust the prior inventory more substantially and to reveal additional local emission features. In contrast, the situation in Chengdu is more complex. The influence of complex terrain and unstable meteorological conditions limits the availability of satellite observations, which in turn leads to a non monotonic relationship among ObsErr, GlobErr, and total emissions. As ObsErr decreases and GlobErr increases, the ten day cumulative CO_2 emissions in Chengdu first decrease and then increase, with inflection behavior occurring near ObsErr of about 1.5 ppm and GlobErr of about 8 megaton per year. This result suggests that when observational uncertainty becomes too large, the inversion system loses effective constraint on the prior estimate and the total emissions tend to return toward the prior value. Similarly, when GlobErr is set to an excessively small value, the system lacks sufficient flexibility to depart from the prior field, which again causes the total emissions to converge toward the prior estimate. Although observational coverage in Chengdu is limited, these response characteristics remain evident and highlight the crucial role of error parameter specification in urban CO_2 emission inversion. When the allowable correction range for total emissions in Xining is excessively large, the inversion yields an overcorrection that converts a carbon source into an apparent carbon sink and produces a negative total emission estimate.

From the perspective of SigTime, the three cities exhibit broadly consistent behavior. As SigTime increases, the ten day cumulative CO_2 emissions progressively diverge from prior levels. This behavior indicates that longer temporal correlation assumptions enhance the ability of the inversion system to represent the cumulative and continuous nature of emission processes and to respond more effectively to actual emission variations. As further illustrated in Fig. 6, when satellite observations provide sufficient coverage of the inversion time window, as in Weifang and Xining, the impact of increasing SigTime gradually stabilizes and the system approaches an adjustment saturation state. When observational coverage is limited, as in Chengdu, the influence of SigTime continues even after partial flattening, which indicates that additional adjustment potential remains.

3.3 Spatial adjustment effects of model parameters

A systematic sensitivity analysis was conducted to assess the influence of the key parameters introduced in Section 2.3 on the spatial distribution of CO_2 fluxes across each of the three cities. In this experiment, the five key parameters were varied within the limits indicated in Table 2. The effects of different parameter settings on the spatial structure and magnitude of CO_2 fluxes were quantitatively evaluated using flux frequency distribution histograms presented in Figure 5.

https://doi.org/10.5194/egusphere-2026-2619
Preprint. Discussion started: 18 June 2026

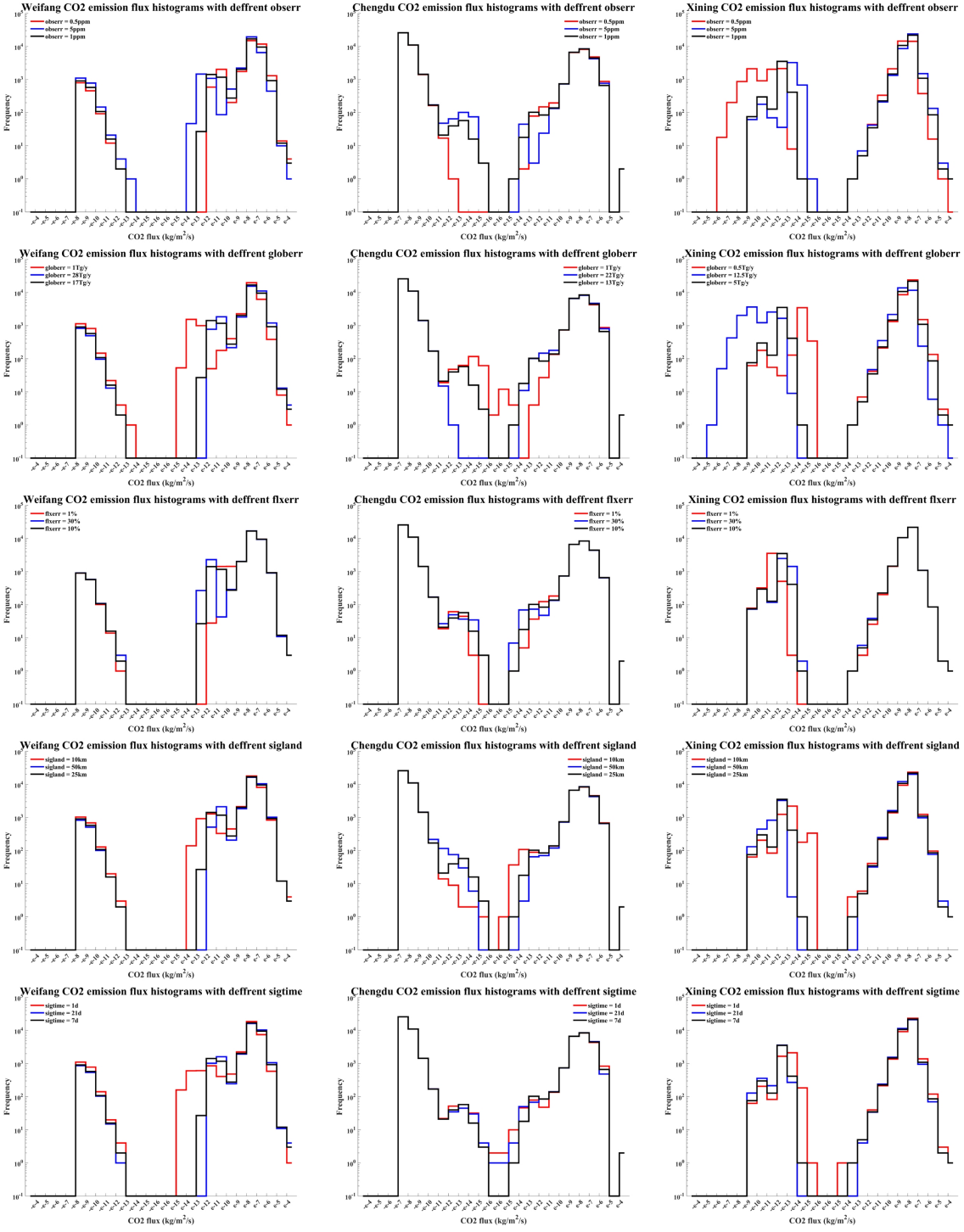

Figure 5: Histograms of CO_2 flux distributions for different parameter configurations in Weifang, Chengdu, and Xining (left to right): effects of ObsErr, GlobErr, FlxErr, SigLand and SigTime (top to bottom). Red, blue, and black lines represent Groups 1, 6, and the standard case, respectively.

https://doi.org/10.5194/egusphere-2026-2619
Preprint. Discussion started: 18 June 2026

Figure 5 presents histograms showing the influence of FlxErr, GlobErr, FlxErr, SigLand and SigTime on CO_2 flux distributions in Weifang, Chengdu, and Xining. Red, blue, and black curves represent results from Exp 1, Exp 6, and default parameter setting, respectively. In Weifang, the flux frequency distribution exhibits a clear bimodal structure, with positive fluxes (emissions) occurring significantly more frequently than negative fluxes (uptake). The emission peak is located between 10^{-8} and 10^{-7} $kg \cdot m^{-2} \cdot s^{-1}$, while the uptake peak lies in the range of -10^{-8} to -10^{-9} $kg \cdot m^{-2} \cdot s^{-1}$. Overall, CO_2 emission magnitudes exceed those of CO_2 sinks. This suggests that the majority of grid cells in Weifang are emission-dominated, with relatively high overall CO_2 output and a significant number of high-emission hotspots. In other words, the CO_2 flux pattern in Weifang is characterized by strong emissions and weak uptake. In contrast, the flux distribution in Chengdu shows that the uptake is stronger than the emissions, i.e. Chengdu is a net sink. The peak of CO_2 uptake is centered around -10^{-7} $kg \cdot m^{-2} \cdot s^{-1}$, while the peak of emissions lies between 10^{-9} and 10^{-8} $kg \cdot m^{-2} \cdot s^{-1}$. The flux distribution in Chengdu is also characterized by a high frequency of near-zero values, indicating weak emission or uptake. High-emission grid cells are relatively sparse. In Xining, the peak of the positive CO_2 flux distribution is around $10^{-8} kg \cdot m^{-2} \cdot s^{-1}$, while that of the negative flux is at approximately $-10^{-12} kg \cdot m^{-2} \cdot s^{-1}$, indicating an overall pattern of weak emissions and weak uptake.

Table 3 Statistical Table of Urban CO_2 Emission and Uptake Differences for Different System Parameters.

Δ err(×10⁵t)		Weifang		Chengdu		Xining	
		emission	uptake	emission	uptake	emission	uptake
ObsErr	**0.5ppm**	10.17	0.01	1.71	0.01	-4.46	-0.46
	5ppm	-14.97	-0.01	5.32	0.01	2.55	0.00
GlobErr	**0.01**	-16.88	-0.01	5.80	0.00	2.64	0.00
	0.25	7.49	0.00	3.95	0.02	-6.36	1.94
FlxErr	**0.01**	0.07	0.00	0.07	0.00	0.00	0.00
	0.3	-0.62	0.00	-0.26	0.00	0.02	0.00
SigLand	**10km**	-0.96	0.00	0.40	0.01	0.68	0.00
	50km	0.10	0.00	-0.11	-0.01	-0.59	0.00
SigTime	**1d**	-10.24	0.00	5.56	0.01	1.83	0.00
	21d	2.93	0.00	-3.58	0.00	-0.86	0.00

Table 3 presents the differences between the total CO_2 emissions and absorptions obtained from Exp 1 and Exp 6 and the corresponding reference values for Weifang, Chengdu, and Xining. Overall, based on the combined analysis of Fig. 5 and Table 3, the differences in total CO_2 absorption in Weifang and Chengdu fluctuate within approximately $\pm 0.01 \times 10^5$ t, indicating that variations in system parameters have a relatively minor impact on carbon sink regions.

As shown in the first column of Fig. 5, in Weifang, ObsErr and GlobErr exert a significant influence on the total CO_2 emissions over a 10-day period, consistent with the findings discussed in Section 3.2. As ObsErr decreases and GlobErr increases, high-emission regions in Weifang (10^{-5} to $10^{-4} kg \cdot m^{-2} \cdot s^{-1}$) intensify markedly, while low-emission regions (10^{-13} to $10^{-11} kg \cdot m^{-2} \cdot s^{-1}$) are significantly diminished, exhibiting a pronounced "seesaw" effect. Variations in FlxErr have little impact on the occurrence frequency of high CO_2 emissions, but they induce noticeable spatial adjustments in the low-emission regions, particularly within the emission range below 10^{-9} $kg \cdot m^{-2} \cdot s^{-1}$. Specifically, as FlxErr increases, the frequency of 10^{-11} $kg \cdot m^{-2} \cdot s^{-1}$ emissions

https://doi.org/10.5194/egusphere-2026-2619
Preprint. Discussion started: 18 June 2026

in the low-emission regions of Weifang decreases, while the frequency of emissions in the 10^{-13} to 10^{-12} $kg \cdot m^{-2} \cdot s^{-1}$ range increases. The influence of SigLand on total emissions is similar to that of FlxErr, but its main effect on flux distribution is to smooth out strong emission areas. As SigLand increases, the strong CO_2 emission regions in Weifang are attenuated. SigTime has a certain influence on the total CO_2 emissions in Weifang, but its impact on the distribution of emission frequencies is relatively minor.

As shown in the second column of Fig. 5, in Chengdu, ObsErr and GlobErr primarily affect CO_2 fluxes in the 10^{-5} and $<10^{-10}$ $kg \cdot m^{-2} \cdot s^{-1}$ ranges, with limited influence on the peak frequency range of emissions. When ObsErr decreases, both high and low emission frequencies increase in Chengdu; however, when ObsErr reaches 5 ppm, low-emission regions are suppressed and shift toward even lower flux values, while high-emission regions are significantly enhanced. When is set to 1×10^6 $t \cdot y^{-1}$, Chengdu exhibits a "seesaw" pattern in CO_2 flux distribution similar to that in Weifang. However, the influence of GlobErr on the CO_2 flux distribution in Chengdu is relatively minor in regions characterized by strong emissions or strong sinks, and is instead concentrated in areas with weak sources and sinks. The effects of FlxErr and SigLand on the CO_2 flux distribution in Chengdu are generally consistent with those observed in Weifang; however, due to Chengdu's complex topography, the responses exhibit greater variability. When SigLand is relatively short (10 km), weak CO_2 uptake regions (-10^{-11} to -10^{-15} $kg \cdot m^{-2} \cdot s^{-1}$) are partially transformed into weak emission regions (10^{-16} to 10^{-14} $kg \cdot m^{-2} \cdot s^{-1}$). The CO_2 flux distribution in Chengdu also shows a smoothing effect with increasing SigTime, but unlike SigLand, the low-emission and low-absorption regions are enhanced at the same time, which may be related to the fact that there is only one track of XCO_2 observations in Chengdu during the assimilation time window.

As shown in the third column of Fig. 5, unlike Weifang and Chengdu, the terrestrial ecosystem in Xining exhibits more substantial adjustments in response to parameter variations. While changes in ObsErr and GlobErr do not significantly alter the peak frequency of CO_2 emission distributions, they exert a marked influence on the frequency distribution of CO_2 uptake in Xining. Similar to Weifang, Xining shows a "seesaw" effect in CO_2 emissions under changes in ObsErr and GlobErr. However, in contrast, a decrease in ObsErr and an increase in GlobErr lead to a significant enhancement in CO_2 uptake in Xining. Given the generally weak CO_2 emission and uptake in Xining, the impacts of FlxErr and SigLand on flux spatial distribution are relatively limited. The influence of SigTime on the CO_2 flux distribution in Xining is also similar to that observed in Weifang, with no significant changes detected.

Overall, ObsErr and GlobErr induce a "seesaw" effect in CO_2 emission distribution. FlxErr primarily influences weak emission regions (less than 10^{-9} $kg \cdot m^{-2} \cdot s^{-1}$), with limited effects on CO_2 uptake zones. SigLand mainly serves to smooth the flux spatial distribution. In regions with complex topography (e.g. Chengdu), a short SigLand may lead to inversions between weak emission and weak uptake areas. SigTime has a notable impact on the total emissions, but its effect on spatial flux patterns is limited when the observation frequency within the assimilation window is sufficient. However, if observation coverage is insufficient, a longer SigLand may distort the spatial distribution of CO_2 fluxes.

https://doi.org/10.5194/egusphere-2026-2619
Preprint. Discussion started: 18 June 2026

3.4 Temporal sensitivity characteristics of model parameters

To further investigate the spatiotemporal response characteristics of urban CO_2 emissions in different cities, we performed 10 day CO_2 flux inversion experiments for Weifang, Chengdu, and Xining. The sensitivity of observed column averaged mixing ratios to preceding emissions was quantified in order to distinguish contributions from local and nonlocal sources. For each satellite observation, the normalized contributions of emissions during the previous seven days were computed and separated into components originating within the inversion domain and components associated with background or remote sources. The corresponding results are presented in Fig. 6.

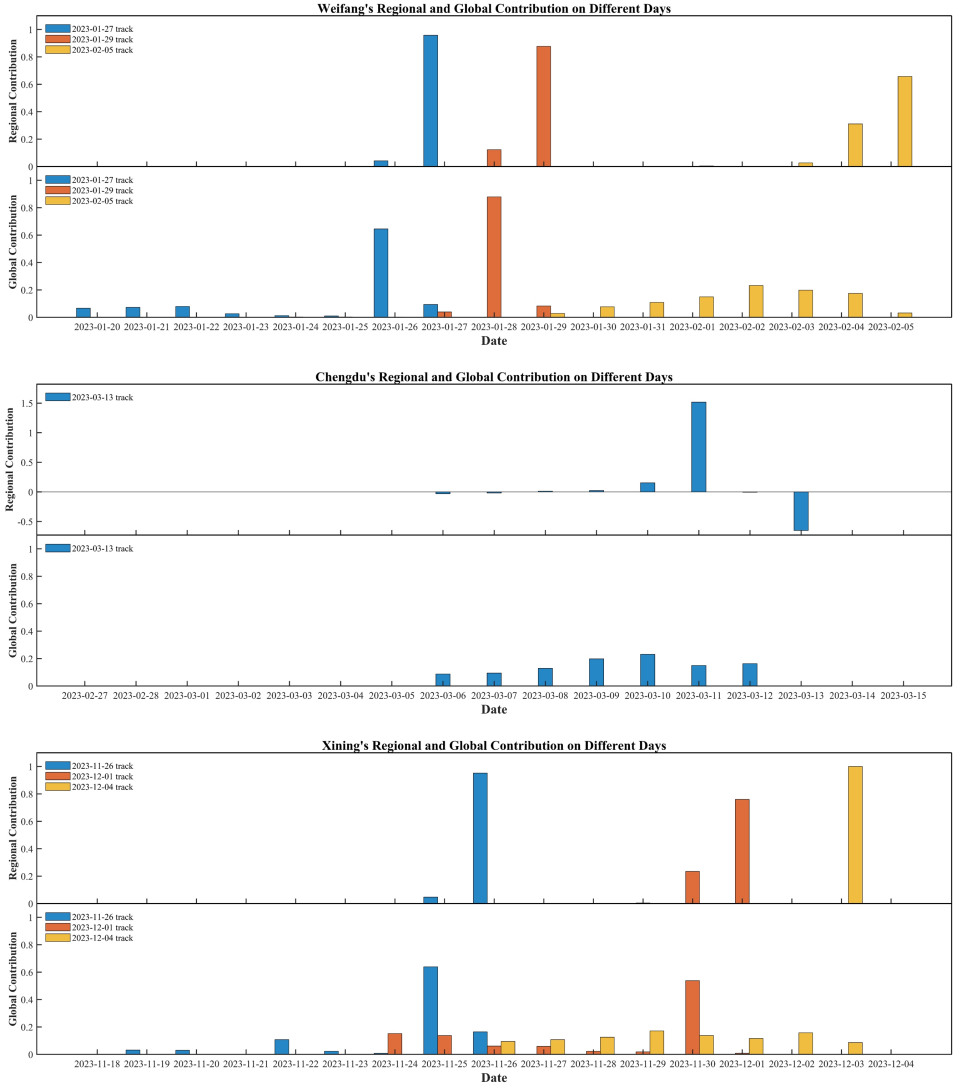

Figure 6 Normalized temporal contributions of emissions from different preceding days to each satellite overpass in Weifang, Chengdu, and Xining. Each color represents a single observation. Upper and lower panels denote contributions from the urban inversion domain and from global and remote sources

https://doi.org/10.5194/egusphere-2026-2619
Preprint. Discussion started: 18 June 2026

Figure 6 presents the normalized temporal contributions of emissions from different preceding days to each satellite overpass for Weifang, Chengdu, and Xining. Each color represents a single observation. The upper part of each panel indicates the influence of emissions within the urban inversion domain, and the lower part represents the contributions from global and remote emission sources. Overall, all three cities exhibit a common pattern in which local emissions dominate the satellite signal, while global emissions exert a more gradual influence. The impact of urban emissions is primarily concentrated within 1 - 3 days prior to observation, rapidly declining over time and exhibiting a clear lagged response. In contrast, the background contribution is more stable and peaks 1 - 2 days earlier, indicating a delayed response of background CO_2 to the observation.

Specifically, in Weifang, the peak contribution from local emissions occurs within one day prior to observation, showing the shortest influence window and the fastest decay rate. This suggests that the satellite signal is mainly affected by high-frequency, near-surface emissions, consistent with the rapid air mass transport facilitated by the open terrain of the North China Plain and prevailing land-sea breezes. The influence of global emissions on Weifang observations is limited, as indicated by the lower and flatter dashed-line profiles.

Specifically, in Weifang, the peak contribution from local emissions occurs within one day prior to observation, showing the shortest influence window and the fastest decay rate. This suggests that the satellite signal is mainly affected by high-frequency, near-surface emissions, consistent with the rapid air mass transport facilitated by the open terrain of the North China Plain and prevailing land-sea breezes. The influence of global emissions on Weifang observations is limited, as indicated by the relatively small contributions in the lower part of the bars.

In Chengdu, both local and global emissions affect the satellite observations over a longer duration compared to Weifang. The normalized contribution from local emissions remains elevated within 2-4 days prior to observation, indicating a more pronounced lag. This pattern can be attributed to Chengdu's geographic position along the western edge of the Sichuan Basin, where low wind speeds and weak atmospheric mixing frequently result in stagnant meteorological conditions that inhibit pollutant dispersion(Liu et al., 2016) and enhance the lagged impact of local emissions on observations. As one of the regions in China with the poorest atmospheric self-cleaning capacity, the Sichuan Basin experiences persistently low average wind speeds(Wang et al., 2020; Xia et al., 2024). This exacerbates the accumulation of pollutants in urban areas and enhances the sensitivity of CO_2 flux inversion to historical emissions, causing satellite observations to remain influenced by prior emissions over extended periods. Additionally, global contributions in Chengdu show relatively small variation compared to local contributions, reinforcing the dominance of in-situ emissions over background perturbations. This phenomenon further confirms that the basin topography constrains external air mass intrusion and atmospheric exchange, resulting in a CO_2 concentration pattern primarily controlled by local sources.

In Xining, the contribution from local emissions resembles that in Weifang, with a peak occurring one day prior to observation, indicating that the satellite signal is predominantly influenced by frequent near-surface emissions. Despite its location in a narrow river valley on the northeastern edge of the Tibetan Plateau, where adjacent mountains significantly constrain wind flow, Xining experiences strong daytime turbulence (up to 3000 m), which facilitates vertical mixing and rapid decay of local CO_2 signals within 24 hours(Maming-Liang et al., 2014; Zhou et al., 2023). Regarding global emissions, Xining lies between

https://doi.org/10.5194/egusphere-2026-2619
Preprint. Discussion started: 18 June 2026

Weifang and Chengdu in terms of temporal influence duration. The complex terrain of the plateau leads to variable transport pathways and active local circulation, resulting in a more evenly distributed and temporally dispersed global emission contribution.

In summary, city geography, terrain closure, and atmospheric transport conditions play a pivotal role in shaping the temporal response characteristics of CO_2 flux inversions. Typically, local contributions influence observations over 1 - 3 days, while global emissions have a slightly longer influence of approximately 3 - 5 days. Complex terrain and calm wind conditions (e.g., in Chengdu) can further extend the period during which this influence is effective. Within the assimilation window, increasing observation frequency helps to capture both local and global emission contributions more effectively, thereby improving the robustness of the flux inversion. Extending SigTime may offer limited benefits if the observational coverage within the window is sparse. Therefore, in urban-scale CO_2 inversions, it is essential to tailor the emission influence window based on local topography and meteorological conditions and to increase the temporal density of observations to improve inversion accuracy.

4 Discussion

4.1 Estimation of global uncertainty

In the implementation of city-scale CO_2 flux inversions using the FEISSO carbon data assimilation system, we identified ObsErr and GlobErr as two critical parameters governing the reliability of emission estimates. These parameters play a dominant role in regional total emission estimation and are fundamental prerequisites for accurately capturing urban CO_2 emission characteristics. By aligning the assumed observational uncertainty with the known uncertainty of the satellite column-averaged CO_2 product, the influence of measurement error on the inversion results can be effectively constrained. Accordingly, properly determining GlobErr is essential for improving the accuracy of the inversion results. Given the temporal lag inherent in inventory-based prior emission estimates, we estimated regional CO_2 flux uncertainty by combining city-level emission intensity growth rates with the discrepancy between historical prior emissions and statistically reported total emissions. We estimated the global uncertainty using the interannual growth rate of CO_2 emissions relative to the Gross City Product (GCP) as follows:

$$\text{globerr} = emission_{year} \times (\text{Growth}_{\text{year}} \times 2 + \text{Difference}_{priori-sata}) \quad (7)$$

where $emission_{year}$ represents the annual CO_2 emissions from the prior inventory, $Growth_{year}$ denotes the city-specific emission intensity growth rate (i.e., CO_2 emissions per unit GDP), and $Difference_{priori\text{-}stat}$ is the relative difference between the prior emissions and statistically reported total emissions. Based on GDP information from the China Urban Statistical Yearbook and emission data from the EDGAR inventory, the emission intensity growth rates for the period 2022 to 2023 were 1.4% lower in Weifang, 0.45% lower in Chengdu, and 4.85% lower in Xining. The discrepancies between the 2022 prior CO_2 emissions and statistics-based totals were -13.9% for Weifang and 1.5% for Xining. City-level statistical data for Chengdu in 2022 were not available at the time of analysis. Following Equation (7), we defined the regional CO_2 flux uncertainty as the

https://doi.org/10.5194/egusphere-2026-2619
Preprint. Discussion started: 18 June 2026

sum of twice the emission intensity growth rate and the known deviation between prior and statistical totals. Consequently, the domain-level CO_2 flux uncertainty was set to 16.7% and 11.2% of the annual total emissions for Weifang and and 11.2% of that for Xining. For Chengdu, in the absence of recent local statistics, a fixed uncertainty of 15% was adopted based on sensitivity analysis results.

4.2 Estimation of total emissions

To further investigate how geographical differences and stages of urban development affect CO_2 flux inversion characteristics, we recommend model parameters for Weifang, Chengdu, and Xining based on a comprehensive evaluation of parameter sensitivities (Sections 3 and 4.1), as summarized in Table 4.

Table 4 Table of System Parameter Settings for Weifang, Chengdu, and Xining.

	ObsErr (ppm)	GlobErr (t)	FlxErr	SigLand (km)	SigTime (day)
Weifang	1.0	$16.7\% \times emission_{year}$	10%	25	3
Chengdu	1.0	$15\% \times emission_{year}$	10%	25	7
Xining	1.0	$11.2\% \times emission_{year}$	10%	25	3

FEISSO was used with these parameters to estimate the 10-day total CO_2 emissions for Weifang, Chengdu, and Xining. The contributions from the terrestrial ecosystem in the prior fluxes account for -5.26%, -111%, and 11.3%. The fossil fuel CO_2 emissions obtained after removing the influence of terrestrial ecosystem fluxes, including comparisons with prior inventory and local statistical data, as well as the spatial distribution patterns, are presented in Fig. 7. The estimated 10-day fossil fuel CO_2 emissions were 3.09×10^6 t for Weifang, 2.19×10^6 t for Chengdu, and 0.57×10^6 t for Xining. A comparison of fossil fuel CO_2 emissions in Weifang, Chengdu, and Xining is presented in Table 5.

Table 5 Statistical summary of fossil fuel CO_2 emissions in Weifang, Chengdu, and Xining.

$CO_2(\times10^6$ t)	Total	NPP	Anthro	EDGAR	Local	Wang 2019	MODIS NPP
Weifang	3	-0.09	3.09	3.6	3.02	-	-0.15
Chengdu	0.6	-1.52	2.19	1.15	-	1.7	-1.09
Xining	0.67	0.1	0.57	0.66	0.64	1.16	0.00

As a representative industrial city, Weifang contains a large number of traditional high carbon industries (Ma et al., 2024). Although the GDP of Weifang is lower than the GDP of Chengdu, the CO_2 emission intensity per unit GDP is substantially higher, which leads to the highest total CO_2 emissions among the three cities as shown by the inversion results. Emission hotspots in Weifang are spatially extensive and intense, and they show strong sensitivity to model parameters such as prior flux uncertainty and spatial correlation length. In contrast, Chengdu has the highest total economic output among the three cities. The rapid expansion of green and low carbon industries, including renewable energy and information technology, has reduced the share of traditional high carbon sectors in recent years (Xiao et al., 2024; Yu et al., 2024), which results in overall

https://doi.org/10.5194/egusphere-2026-2619
Preprint. Discussion started: 18 June 2026

lower CO_2 emissions than in Weifang. Chengdu is located in the central Sichuan Basin, where low elevation and weak near surface winds suppress atmospheric dispersion and favor the accumulation of pollutants (Chen et al., 2021; Xiong et al., 2023). These conditions limit the effectiveness of flux adjustments over emission hotspot regions and tend to cause local CO_2 mixing ratios to be overestimated. Xining has the lowest GDP and the lowest total CO_2 emissions among the three cities. Emission
585 hotspots in Xining are spatially concentrated and relatively weak in intensity (Zhao et al., 2019), which leads to the lowest parameter sensitivity and indicates strong stability in the inverted flux fields.

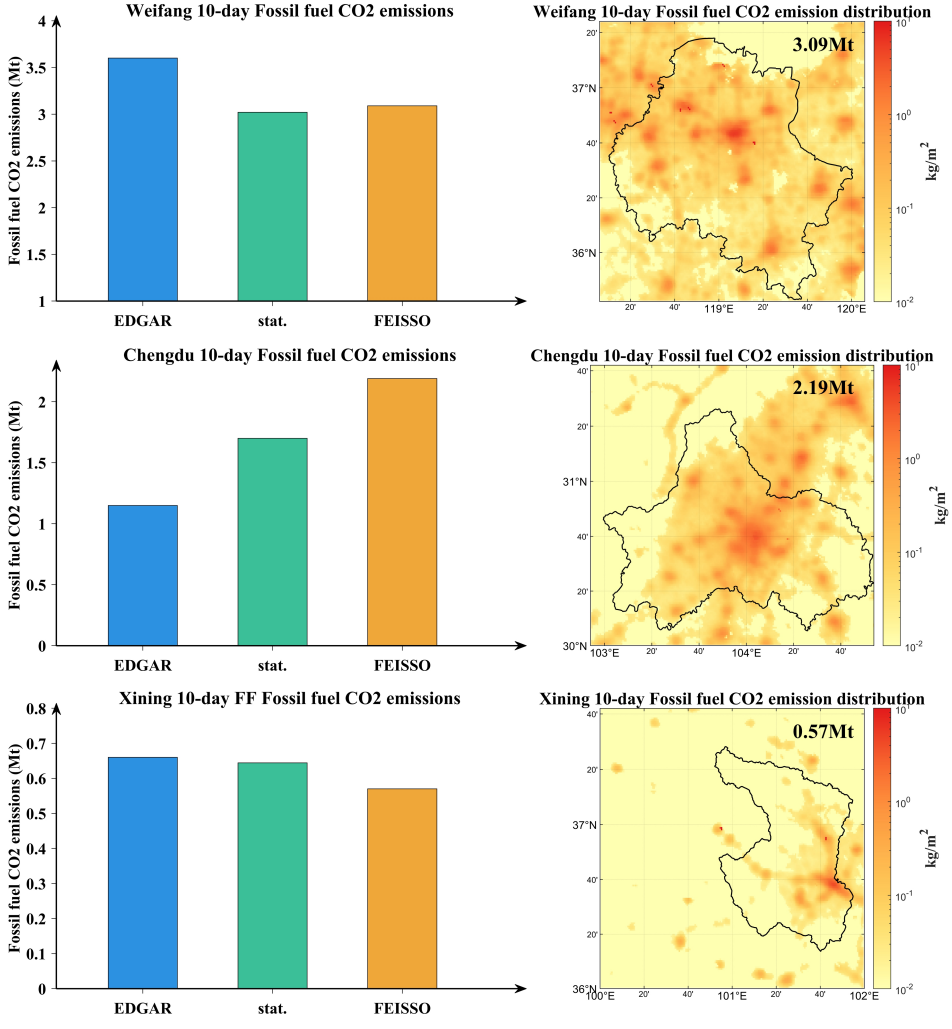

Figure 7. 10-Day Total CO_2 emissions estimated using FEISSO, together with EDGAR inventory and local statistical data (stat.) for Weifang, Chengdu, and Xining (left) and spatial distributions of the FEISSO fossil fuel CO_2 emissions over these cities (right)

590 The uncertainty in CO_2 flux estimation primarily arises from the quantity and temporal frequency of satellite-based column-averaged CO_2 (XCO_2) observations. Due to the orbital limitations of the OCO-2 satellite, consistent observational coverage cannot be guaranteed within a 10-day assimilation window. Wu et al. (2020) highlighted that satellite observations with high

https://doi.org/10.5194/egusphere-2026-2619
Preprint. Discussion started: 18 June 2026

temporal frequency and wide spatial coverage can significantly enhance the reliability of urban-scale CO_2 flux assimilation (Wu et al., 2023). To maximize observational coverage during the assimilation window, we examined all satellite overpasses over the three urban regions in 2023. We found that both Weifang and Xining received data from three orbital tracks within each 10-day window, with a total of 829 and 676 valid observations, respectively. In contrast, due to sparser coverage, the selected assimilation window in this study represents the time period with the highest number of valid observations available for Chengdu. Although the limited number of satellite tracks may introduce radial-pattern uncertainties in hotspot emission regions, sensitivity analysis for Chengdu indicates that this effect does not significantly impact the overall spatial distribution or total regional emissions, and the trends in response to parameter variations remain consistent.

4.3 Evaluation of emission hotspot impacts

By comparing the inversion results obtained under different parameter configurations, particularly the posterior flux distributions, we find that the spatial locations of the major emission hotspots remain largely stable. The differences are mainly reflected in the adjustments to emission magnitudes. To further assess the ability of FEISSO to identify point source emissions, we selected two identified plumes from CarbonMapper over Weifang on 29 March 2024. Figure 8 shows the superimposed display of our posterior flux distribution, the local point emission, and the plumes identified by CarbonMapper. The prior flux distributions used for inversion are redistributed to the EDGAR fossil fuel sectors by the ODIAC emissions (Fig. 8a & b) and the local point emission inventories (Fig. 8c, d). For local point emissions, the size of the red points indicates the emission intensity, and the exact values are marked on the Fig. 8. The plumes form CarbonMapper are located at 118.774°E, 36.93°N and 118.907°E, 37.268°N. The CO_2 flux from CarbonMapper and our study have been converted to the same unit and their intensity is indicated with a consistent color bar. According to the local emission inventory of Weifang, plume 1 is mainly associated with Shandong Shouguang Juneng Special Steel Co., Ltd. and the First Branch of Shandong Lianmeng Chemical Co., Ltd. Plume 2 is primarily related to Shenhua Guohua Shouguang Power Co., Ltd.

The ODIAC-based point-source emission map for Weifang presented in Fig. 8a & b indicates substantial spatial discrepancies in the location of emission hotspots. The FEISSO inversion results depend strongly on the spatial structure of the prior emission inventory. Using the locations of the maximum values in the ODIAC-based posterior fields as the spatial reference, the distances between the plume locations identified by CarbonMapper and the two maximum value centers are 1.85 km and 5.55 km, which indicates a pronounced spatial discrepancy. This phenomenon is mainly attributed to the spatial allocation strategy of ODIAC, which relies on nighttime light data in urban areas. Industrial sources have relatively weak nighttime radiation signals, which leads to a systematic displacement in the representation of large industrial point sources. In addition, point sources exhibit high emission intensity, but their spatial positions are difficult to fully constrain during the inversion process. As a result, the posterior fields tend to show overly diffused emission areas and weakened emission centers. Furthermore, in Fig. 8b, the point source associated with Weifang Zhenxing Coking Co Ltd is not matched with a corresponding plume signal in the CarbonMapper data. This further indicates that the joint constraint between observations and emission inventories is insufficient for some industrial emission sources. Overall, obtaining a more accurate and physically consistent spatial

https://doi.org/10.5194/egusphere-2026-2619
Preprint. Discussion started: 18 June 2026

distribution of urban CO_2 emissions is of substantial scientific importance for identifying and characterizing urban emission hotspots and for improving the monitoring and inversion capability for point sources.

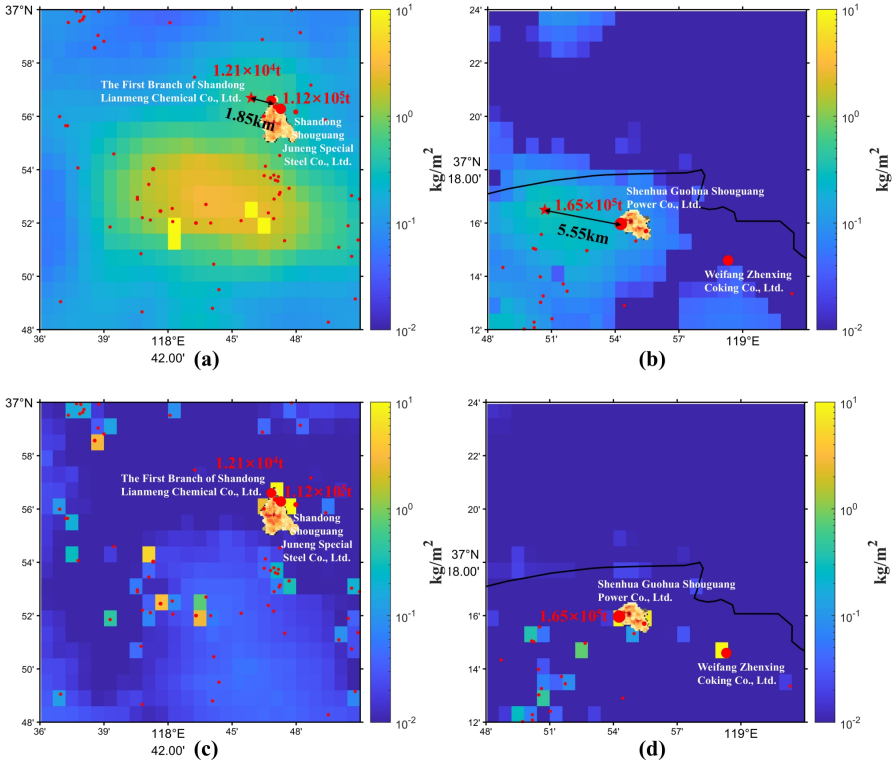

Figure 8 Performance of FEISSO at the point-source scale under ODIAC and local CO_2 emission inventory spatial distributions. (a) and (b) show the results for plume 1 and plume 2 with the ODIAC spatial distribution; (c) and (d) show the corresponding results with the local emission inventory spatial distribution

Based on this consideration, we used the city-level total emissions from EDGAR as a constraint and redistributed Weifang's 2023 EDGAR emissions according to the spatial distribution of local point sources. This produced a more accurate prior inventory for point-source emissions, which was then used for the inversion of 10-day CO_2 fluxes in Weifang. The inversion results using the revised prior informed by the local inventory are shown in Fig. 8 c & d. The changes in point-source emissions before and after adjusting the spatial distribution of the prior, as well as comparisons with the local inventory and CarbonMapper, are summarized in Table 6. After incorporating the local emission inventory and applying spatial distribution corrections, the emission estimates for plume 1 and plume 2 increased from 333.36 t and 144.37 t in the ODIAC-based results to 1.64×10^5 t and 2.00×10^5 t. Their differences relative to the local inventory decreased from -99.7% and -99.9% to 33.3% and 21.2%, which substantially reduced the relative error over the emission hotspot regions. In terms of relative deviation from the local inventory, the local corrected results also show more than 50% improvement over CarbonMapper for the two plume regions. With respect to spatial location, the posterior hotspot location error of the Local-corrected results decreased from 1.85 km and 5.55 km in the ODIAC-based case to 1.12 km and 0.37 km when compared with CarbonMapper observations,

https://doi.org/10.5194/egusphere-2026-2619
Preprint. Discussion started: 18 June 2026

indicating a clear enhancement in hotspot location accuracy. Overall, location based and structural corrections of prior emission inventories using local information are of substantial scientific importance for improving the identification of urban emission hotspots and enhancing the accuracy of quantitative emission estimation.

Table 6 Comparison of point-source emissions before and after correcting the spatial distribution of the prior inventory.

			plume1	plume2
Local inventory			1.23×10^5	1.65×10^5
CO_2 emission flux (t)	FEISSO	ODIAC-based	333.36	144.37
		Local-corrected	1.64×10^5	2.00×10^5
	CarbonMapper		$3.55\pm1.24\times10^4$	$9.42\pm1.11\times10^4$
Relative Errors (%)	FEISSO	ODIAC-based	-99.7%	-99.9%
		Local-corrected	33.3%	21.2%
	CarbonMapper		-71.1%	-42.9%
location error relative to CarbonMapper (km)	FEISSO	ODIAC-based	1.85	5.55
		Local-corrected	1.12	0.37

After applying a refined spatial correction to the emission distribution in Weifang, the ten day total CO_2 emissions were estimated at 3.03×10^6 t, which is slightly lower than the 3.09×10^6 t obtained from the ODIAC-based results and closer to the ten day total reported in the local inventory of 3.02×10^6 t. This result indicates that correcting the spatial distribution of prior emission inventories using local information can substantially improve the reliability and consistency of high resolution urban CO_2 flux inversion. It also highlights the critical role of prior inventory spatial accuracy in constraining inversion results.

In summary, correcting the spatial distribution of CO_2 point-source emissions significantly reduces the systematic biases in FEISSO-derived point-source estimates. Additional experiments confirm that the model is capable of effectively detecting and quantifying emissions from large industrial point sources even at kilometre-scale spatial resolution. These findings indicate that FEISSO-Carbon has strong capability in identifying and correcting emission characteristics in complex regions. The model is particularly suitable for monitoring and quantifying major industrial point sources in heavily industrialized areas, and it provides high accuracy and reliability in both point-source detection and emission estimation.

5 Conclusion

In this study, we developed an urban-scale carbon flux inversion system, FEISSO, which integrates a Lagrangian atmospheric transport model with a Bayesian assimilation framework to explore the feasibility of retrieving high resolution urban CO_2 flux distributions from satellite XCO_2 observations. Sensitivity experiments were conducted for Weifang, Chengdu, and Xining,

https://doi.org/10.5194/egusphere-2026-2619
Preprint. Discussion started: 18 June 2026

which differ in geographic location and economic development, to identify the key factors affecting the accuracy and robustness of urban-scale CO_2 flux inversion.

In the study, we first examined the impact of transport model resolution on urban-scale CO_2 flux inversion by comparing trajectory simulations using meteorological data with resolutions of 1° and 0.25° . The results show that the spatial resolution of meteorological fields strongly affects the ability of transport models to resolve CO_2 trajectories. Higher resolution forcing substantially improves simulation accuracy and enhances the capacity to capture spatial details in flux distributions. Using the 0.25° resolution setup, sensitivity analyses were conducted for five key inversion parameters: column averaged CO_2 observation error (ObsErr), total error for the inversion domain (GlobErr), prior flux error (FlxErr), land spatial correlation length (SigLand), and temporal correlation length (SigTime).

Results indicate that ObsErr and GlobErr are the primary factors influencing total urban CO_2 emission estimates, followed by SigTime. FlxErr and SigLand exert weaker effects on total emissions. In terms of spatial adjustment, ObsErr and GlobErr induce a seesaw pattern in flux distributions. FlxErr contributes to fine structural adjustment, mainly in vegetated areas with low emissions, while SigLand primarily smooths the flux distribution. When observational coverage within the assimilation window is sufficient, the effect of SigTime on spatial flux distribution becomes negligible. Observation frequency, topographic complexity, and meteorological stability jointly shape the temporal response of CO_2 flux inversion, leading to pronounced intercity variability.

Based on the understanding of these mechanisms, this study provides parameter setting recommendations tailored to the characteristics of each city. After optimizing the parameter configuration, the FEISSO system successfully inverted ten day CO_2 emissions for Weifang, Chengdu, and Xining, yielding totals of 3.09×10^6 t, 2.19×10^6 t, and 0.57×10^6 t, respectively. The inversion results for Weifang and Xining show good agreement with EDGAR emissions and local statistical data, validating the applicability and stability of the system.

The results form this study demonstrate the potential of FEISSO for broader application. The frequency of urban-scale inversions is limited by the current OCO-2 satellite coverage. With continued improvements in satellite observation frequency, orbital design, and data accuracy, FEISSO is expected to play an increasingly important role in monitoring urban carbon emissions, evaluating mitigation policies, and supporting refined global urban carbon management.

Data availability

The FEISSO demonstration dataset used in this study is publicly available on Zenodo at https://doi.org/10.5281/zenodo.20073187 (Yao et al., 2026).

https://doi.org/10.5194/egusphere-2026-2619
Preprint. Discussion started: 18 June 2026

Author contributions

Xingyu Yao: Xingyu Yao: Writing-original draft, Methodology, Validation; Ying Zhang: Writing-original draft, Methodology, Formal analysis, Conceptualization; Xiaofan Li: Methodology; Gerrit de Leeuw: Funding acquisition, Review & editing; Cheng Fan: Funding acquisition; Yuanxun Zhang, Zhanshan Wang, Yongjie Wei: Resources; Zhengqiang Li: Methodology, Supervision. All authors reviewed and approved the final manuscript.

Competing interests

The authors declare that they have no competing interests.

Disclaimer

Copernicus Publications remains neutral with regard to jurisdictional claims made in the text, published maps, institutional affiliations, or any other geographical representation in this paper. While Copernicus Publications makes every effort to include appropriate place names, the final responsibility lies with the authors. Views expressed in the text are those of the authors and do not necessarily reflect the views of the publisher.

Acknowledgements

The authors acknowledge the NASA Goddard Earth Sciences Data and Information Services Center (GES DISC) for providing access to the OCO-2 satellite data, the National Centers for Environmental Prediction (NCEP) for supplying the FNL meteorological data, the Emissions Database for Global Atmospheric Research (EDGAR) for providing the emission inventory data, and the Open-Data Inventory for Anthropogenic Carbon dioxide (ODIAC) for supplying the fossil fuel emission data used in this study.

Financial support

This research was funded by the National Key R&D Program of China, grant number 2023YFB3907405.

References

Ahn, D. Y., Goldberg, D. L., Coombes, T., Kleiman, G., and Anenberg, S. C.: CO2 emissions from C40 cities: citywide emission inventories and comparisons with global gridded emission datasets, Environmental Research Letters, 18, 034032, 10.1088/1748-9326/acbb91, 2023.

https://doi.org/10.5194/egusphere-2026-2619
Preprint. Discussion started: 18 June 2026

Aigner, P., Chen, J., Böhm, F., Chariot, M., Emmenegger, L., Frölich, L., Grange, S., Kühbacher, D., Kürzinger, K., Laurent, O., Makowski, M., Rubli, P., Schmitt, A., and Wenzel, A.: ACROPOLIS: Munich urban CO2 sensor network, Atmos. Meas. Tech., 19, 745–773, 10.5194/amt-19-745-2026, 2026.

Beer, C., Reichstein, M., Tomelleri, E., Ciais, P., Jung, M., Carvalhais, N., Rödenbeck, C., Arain, M. A., Baldocchi, D., and Bonan, G. B.: Terrestrial gross carbon dioxide uptake: global distribution and covariation with climate, Science, 329, 834–838, 2010.

Bertelli, M., Cristiana Palazzo, A., Gibertoni, C., Rainaldi, F., and Gaspari, J.: Toward sustainable urban health: defining hospital outdoor spaces for community well-being, IOP Conference Series: Earth and Environmental Science, 1402, 012056, 10.1088/1755-1315/1402/1/012056, 2024.

Chen, S., Xie, Z., Xie, J., Liu, B., Jia, B., Qin, P., Wang, L., Wang, Y., and Li, R.: Impact of urbanization on thermal environment of Chengdu-Chongqing Urban Agglomeration under complex terrain, Earth System Dynamics Discussions, 2021, 1–24, 2021.

Chevallier, F., Remaud, M., O'Dell, C. W., Baker, D., Peylin, P., and Cozic, A.: Objective evaluation of surface- and satellite-driven carbon dioxide atmospheric inversions, Atmos. Chem. Phys., 19, 14233–14251, 10.5194/acp-19-14233-2019, 2019.

Chevallier, F., Fisher, M., Peylin, P., Serrar, S., Bousquet, P., Bréon, F. M., Chedin, A., and Ciais, P.: Inferring CO2 sources and sinks from satellite observations: Method and application to TOVS data, Journal of Geophysical Research: Atmospheres, 110, 2005.

Connor, B. J., Boesch, H., Toon, G., Sen, B., Miller, C., and Crisp, D.: Orbiting Carbon Observatory: Inverse method and prospective error analysis, Journal of Geophysical Research: Atmospheres, 113, https://doi.org/10.1029/2006JD008336, 2008.

Crippa, M., Guizzardi, D., Pagani, F., Schiavina, M., Melchiorri, M., Pisoni, E., Graziosi, F., Muntean, M., Maes, J., Dijkstra, L., Van Damme, M., Clarisse, L., and Coheur, P.: Insights into the spatial distribution of global, national, and subnational greenhouse gas emissions in the Emissions Database for Global Atmospheric Research (EDGAR v8.0), Earth Syst. Sci. Data, 16, 2811–2830, 10.5194/essd-16-2811-2024, 2024.

Crisp, D., O'Dell, C., Eldering, A., Fisher, B., Oyafuso, F., Payne, V., Drouin, B., Toon, G., Laughner, J., and Somkuti, P.: Orbiting Carbon Observatory (OCO-2) Level 2 Full Physics Algorithm Theoretical Basis Document, Version 3.0–Rev 1, NASA, Pasadena, CA, USA, Tech. Rep, 2021.

Detling, J., Parton, W., and Hunt, H.: An empirical model for estimating CO2 exchange of Bouteloua gracilis (HBK) Lag. in the shortgrass prairie, Oecologia, 33, 137–147, 1978.

Friedlingstein, P., O'Sullivan, M., Jones, M. W., Andrew, R. M., Hauck, J., Landschützer, P., Le Quéré, C., Li, H., Luijkx, I. T., Olsen, A., Peters, G. P., Peters, W., Pongratz, J., Schwingshackl, C., Sitch, S., Canadell, J. G., Ciais, P., Jackson, R. B., Alin, S. R., Arneth, A., Arora, V., Bates, N. R., Becker, M., Bellouin, N., Berghoff, C. F., Bittig, H. C., Bopp, L., Cadule, P., Campbell, K., Chamberlain, M. A., Chandra, N., Chevallier, F., Chini, L. P., Colligan, T., Decayeux, J., Djeutchouang, L. M., Dou, X., Duran Rojas, C., Enyo, K., Evans, W., Fay, A. R., Feely, R. A., Ford, D. J., Foster, A., Gasser, T., Gehlen, M., Gkritzalis, T., Grassi, G., Gregor, L., Gruber, N., Gürses, Ö., Harris, I., Hefner, M., Heinke, J., Hurtt, G. C., Iida, Y., Ilyina, T., Jacobson, A. R., Jain, A. K., Jarníková, T., Jersild, A., Jiang, F., Jin, Z., Kato, E., Keeling, R. F., Klein Goldewijk, K., Knauer, J., Korsbakken, J. I., Lan, X., Lauvset, S. K., Lefèvre, N., Liu, Z., Liu, J., Ma, L., Maksyutov, S., Marland, G., Mayot, N., McGuire, P. C., Metzl, N., Monacci, N. M., Morgan, E. J., Nakaoka, S.-I., Neill, C., Niwa, Y., Nützel, T., Olivier, L., Ono, T., Palmer, P. I., Pierrot, D., Qin, Z., Resplandy, L., Roobaert, A., Rosan, T. M., Rödenbeck, C., Schwinger, J., Smallman, T. L., Smith, S. M., Sospedra-Alfonso, R., Steinhoff, T., Sun, Q., Sutton, A. J., Séférian, R., Takao, S., Tatebe, H., Tian, H., Tilbrook, B., Torres, O., Tourigny, E., Tsujino, H., Tubiello, F., van der Werf, G., Wanninkhof, R., Wang, X., Yang, D., Yang, X., Yu, Z., Yuan, W., Yue, X., Zaehle, S., Zeng, N., and Zeng, J.: Global Carbon Budget 2024, Earth System Science Data, 17, 965–1039, 10.5194/essd-17-965-2025, 2025.

Giovannini, L., Antonacci, G., Zardi, D., Laiti, L., and Panziera, L.: Sensitivity of Simulated Wind Speed to Spatial Resolution over Complex Terrain, Energy Procedia, 59, 323–329, https://doi.org/10.1016/j.egypro.2014.10.384, 2014.

Hamilton, S. D., Wu, D., Johnson, M. S., Turner, A. J., Fischer, M. L., Dadheech, N., and Jeong, S.: Estimating Carbon Dioxide Emissions in Two California Cities Using Bayesian Inversion and Satellite Measurements, Geophysical Research Letters, 51, e2024GL111150, https://doi.org/10.1029/2024GL111150, 2024.

Han, P., Yao, B., Cai, Q., Chen, H., Sun, W., Liang, M., Zhang, X., Zhao, M., Martin, C., Liu, Z., Ye, H., Wang, P., Li, Y., and Zeng, N.: Support Carbon Neutral Goal with a High-Resolution Carbon Monitoring System in Beijing, Bulletin of the American Meteorological Society, 105, E2461–E2481, https://doi.org/10.1175/BAMS-D-23-0025.1, 2024.

https://doi.org/10.5194/egusphere-2026-2619
Preprint. Discussion started: 18 June 2026

Hebbert, M.: Cities and Climate Change (Global Report on Human Settlements 2011), 2012.
Hu, K., Feng, X., Zhang, Q., Shao, P., Liu, Z., Xu, Y., Wang, S., Wang, Y., Wang, H., Di, L., and Xia, M.: Review of Satellite Remote Sensing of Carbon Dioxide Inversion and Assimilation, Remote Sensing, 16, 3394, 2024.
Jacobson, A. R., Schuldt, K. N., Tans, P., Arlyn, A., Miller, J. B., Oda, T., Mund, J., Weir, B., Ott, L., Aalto, T., Abshire, J. B., Aikin, K., Aoki, S., Apadula, F., Arnold, S., Baier, B., Bartyzel, J., Beyersdorf, A., Biermann, T., Biraud, S. C., Boenisch, H., Brailsford, G., Brand, W. A., Chen, G., Huilin, C., Lukasz, C., Clark, S., Colomb, A., Commane, R., Conil, S., Couret, C., Cox, A., Cristofanelli, P., Cuevas, E., Curcoll, R., Daube, B., Davis, K. J., De Wekker, S., Coletta, J. D., Delmotte, M., DiGangi, E., DiGangi, J. P., Di Sarra, A. G., Dlugokencky, E., Elkins, J. W., Emmenegger, L., Shuangxi, F., Fischer, M. L., Forster, G., Frumau, A., Galkowski, M., Gatti, L. V., Gehrlein, T., Gerbig, C., Francois, G., Gloor, E., Gomez-Trueba, V., Goto, D., Griffis, T., Hammer, S., Hanson, C., Haszpra, L., Hatakka, J., Heimann, M., Heliasz, M., Hensen, A., Hermansen, O., Hintsa, E., Holst, J., Ivakhov, V., Jaffe, D. A., Jordan, A., Joubert, W., Karion, A., Kawa, S. R., Kazan, V., Keeling, R. F., Keronen, P., Kneuer, T., Kolari, P., Kateřina, K., Kort, E., Kozlova, E., Krummel, P., Kubistin, D., Labuschagne, C., Lam, D. H. Y., Lan, X., Langenfelds, R. L., Laurent, O., Laurila, T., Lauvaux, T., Lavric, J., Law, B. E., Lee, J., Lee, O. S. M., Lehner, I., Lehtinen, K., Leppert, R., Leskinen, A., Leuenberger, M., Levin, I., Levula, J., Lin, J., Lindauer, M., Loh, Z., Lopez, M., Luijkx, I. T., Lunder, C. R., Machida, T., Mammarella, I., Manca, G., Manning, A., Manning, A., Marek, M. V., Martin, M. Y., Matsueda, H., McKain, K., Meijer, H., Meinhardt, F., Merchant, L., Mihalopoulos, N., Miles, N. L., Miller, C. E., Mitchell, L., Mölder, M., Montzka, S., Moore, F., Moossen, H., Morgan, E., Josep-Anton, M., Morimoto, S., Müller-Williams, J., Munger, J. W., Munro, D., Myhre, C. L., Shin-Ichiro, N., Jaroslaw, N., Newman, S., Nichol, S., Niwa, Y., Obersteiner, F., O'Doherty, S., Paplawsky, B., Peischl, J., Peltola, O., Piacentino, S., Jean-Marc, P., Pickers, P., Piper, S., Pitt, J., Plass-Dülmer, C., Platt, S. M., Prinzivalli, S., Ramonet, M., Ramos, R., Reyes-Sanchez, E., Richardson, S. J., Riris, H., Rivas, P. P., Ryerson, T., Saito, K., Sargent, M., Sasakawa, M., Scheeren, B., Schuck, T., Schumacher, M., Seifert, T., Sha, M. K., Shepson, P., Shook, M., Sloop, C. D., Smith, P., Stanley, K., Steinbacher, M., Stephens, B., Sweeney, C., Thoning, K., Timas, H., Torn, M., Tørseth, K., Trisolino, P., Turnbull, J., Van Den Bulk, P., Van Dinther, D., Vermeulen, A., Viner, B., Vitkova, G., Walker, S., Watson, A., Wofsy, S. C., Worsey, J., Worthy, D., Dickon, Y., Zaehle, S., Zahn, A., and Miroslaw, Z.: CarbonTracker CT2022, 10.25925/Z1GJ-3254, 2023.
Jiang, F., Wang, H., Chen, J. M., Ju, W., Tian, X., Feng, S., Li, G., Chen, Z., Zhang, S., and Lu, X.: Regional CO 2 fluxes from 2010 to 2015 inferred from GOSAT XCO 2 retrievals using a new version of the Global Carbon Assimilation System, Atmospheric Chemistry and Physics, 21, 1963–1985, 2021.
Jin, Z., Wang, T., Zhang, H., Wang, Y., Ding, J., and Tian, X.: Constraint of satellite CO2 retrieval on the global carbon cycle from a Chinese atmospheric inversion system, Science China Earth Sciences, 66, 609–618, 2023.
Kunik, L., Mallia, D. V., Gurney, K. R., Mendoza, D. L., Oda, T., and Lin, J. C.: Bayesian inverse estimation of urban CO2 emissions: Results from a synthetic data simulation over Salt Lake City, UT, Elem Sci Anth, 7, 36, 2019.
Kunz, A. K., Hammer, S., Aigner, P., Bignotti, L., Borchardt, L., Chen, J., Della Coletta, J., Emmenegger, L., Eritt, M., Gutiérrez, X., Hashemi, J., Hilland, R., Holst, C., Jordan, A., Kljun, N., Kneißl, R., Lan, C., Legendre, V., Levin, I., Loubet, B., Mauder, M., Molinier, B., Preunkert, S., Ramonet, M., Stagakis, S., and Christen, A.: 14C-based separation of fossil and non-fossil CO2 fluxes in cities using relaxed eddy accumulation: results from tall-tower measurements in Zurich, Paris, and Munich, Atmos. Chem. Phys., 26, 4967–5003, 10.5194/acp-26-4967-2026, 2026.
Kuo, C., Lindberg, C., and Thomson, D. J.: Coherence established between atmospheric carbon dioxide and global temperature, Nature, 343, 709–714, 10.1038/343709a0, 1990.
Lauvaux, T., Miles, N. L., Deng, A., Richardson, S. J., Cambaliza, M. O., Davis, K. J., Gaudet, B., Gurney, K. R., Huang, J., and O'Keefe, D.: High-resolution atmospheric inversion of urban CO2 emissions during the dormant season of the Indianapolis Flux Experiment (INFLUX), Journal of Geophysical Research: Atmospheres, 121, 5213–5236, 2016.
Lee, H., Calvin, K., Dasgupta, D., Krinner, G., Mukherji, A., Thorne, P., Trisos, C., Romero, J., Aldunce, P., and Barrett, K.: Climate change 2023: synthesis report. Contribution of working groups I, II and III to the sixth assessment report of the intergovernmental panel on climate change, 2023.
Lian, J., Laurent, O., Chariot, M., Lienhardt, L., Ramonet, M., Utard, H., Lauvaux, T., Bréon, F. M., Broquet, G., Cucchi, K., Millair, L., and Ciais, P.: Development and deployment of a mid-cost CO2 sensor monitoring network to support atmospheric inverse modeling for quantifying urban CO2 emissions in Paris, Atmos. Meas. Tech., 17, 5821–5839, 10.5194/amt-17-5821-2024, 2024.

https://doi.org/10.5194/egusphere-2026-2619
Preprint. Discussion started: 18 June 2026

Liu, Q., Wang, Z.-W., Ye, Q.-R., Zhou, D.-P., Deng, X., Hu, L., and Yin, H.-L.: The influence of the weather conditions on main atmospheric pollutants concentration in Chengdu, 2016/08, 513–518, 10.2991/eesed-16.2017.71,
Liu, Z., Zeng, N., Liu, Y., Kalnay, E., Asrar, G., Wu, B., Cai, Q., Liu, D., and Han, P.: Improving the joint estimation of CO2 and surface carbon fluxes using a constrained ensemble Kalman filter in COLA (v1.0), Geosci. Model Dev., 15, 5511–5528, 10.5194/gmd-15-5511-2022, 2022.
Ma, L., Wang, C., Xiang, L., Liu, J., Dang, C., and Wu, H.: Chinese cities show different trend toward carbon peak, Science of The Total Environment, 934, 173156, https://doi.org/10.1016/j.scitotenv.2024.173156, 2024.
MAMing-liang, Q., SHEN, H.-y., and ZHANG, J.-k.: Research on the characteristics of wind and thermal field for atmospheric boundary layer in Xining, Journal of Natural Resources, 29, 1196–1206, 2014.
Masson-Delmotte, V., Zhai, P., Pörtner, H.-O., Roberts, D., Skea, J., Shukla, P. R., Pirani, A., Moufouma-Okia, W., Péan, C., and Pidcock, R.: Global warming of 1.5 C, An IPCC Special Report on the impacts of global warming of, 1, 43–50, 2018.
Nations, U.: United Nations Department of Economic and social affairs, Sustainable development goal, 2, 2019.
Nickless, A., Rayner, P. J., Scholes, R. J., Engelbrecht, F., and Erni, B.: An atmospheric inversion over the city of Cape Town: sensitivity analyses, Atmospheric Chemistry and Physics, 19, 7789–7816, 2019.
O'dell, C. W., Eldering, A., Wennberg, P. O., Crisp, D., Gunson, M. R., Fisher, B., Frankenberg, C., Kiel, M., Lindqvist, H., and Mandrake, L.: Improved retrievals of carbon dioxide from Orbiting Carbon Observatory-2 with the version 8 ACOS algorithm, Atmospheric Measurement Techniques, 11, 6539–6576, 2018.
Oda, T., Maksyutov, S., and Andres, R. J.: The Open-source Data Inventory for Anthropogenic CO 2, version 2016 (ODIAC2016): a global monthly fossil fuel CO 2 gridded emissions data product for tracer transport simulations and surface flux inversions, Earth System Science Data, 10, 87–107, 2018.
Peters, W., Jacobson, A. R., Sweeney, C., Andrews, A. E., Conway, T. J., Masarie, K., Miller, J. B., Bruhwiler, L. M., Pétron, G., and Hirsch, A. I.: An atmospheric perspective on North American carbon dioxide exchange: CarbonTracker, Proceedings of the National Academy of Sciences, 104, 18925–18930, 2007.
Pisso, I., Sollum, E., Grythe, H., Kristiansen, N. I., Cassiani, M., Eckhardt, S., Arnold, D., Morton, D., Thompson, R. L., Groot Zwaaftink, C. D., Evangeliou, N., Sodemann, H., Haimberger, L., Henne, S., Brunner, D., Burkhart, J. F., Fouilloux, A., Brioude, J., Philipp, A., Seibert, P., and Stohl, A.: The Lagrangian particle dispersion model FLEXPART version 10.4, Geosci. Model Dev., 12, 4955–4997, 10.5194/gmd-12-4955-2019, 2019.
Remaud, M., Chevallier, F., Cozic, A., Lin, X., and Bousquet, P.: On the impact of recent developments of the LMDz atmospheric general circulation model on the simulation of CO2 transport, Geosci. Model Dev., 11, 4489–4513, 10.5194/gmd-11-4489-2018, 2018.
Rödenbeck, C., DeVries, T., Hauck, J., Le Quéré, C., and Keeling, R. F.: Data-based estimates of interannual sea–air CO2 flux variations 1957–2020 and their relation to environmental drivers, Biogeosciences, 19, 2627–2652, 10.5194/bg-19-2627-2022, 2022.
Rödenbeck, C., Bakker, D. C. E., Metzl, N., Olsen, A., Sabine, C., Cassar, N., Reum, F., Keeling, R. F., and Heimann, M.: Interannual sea–air CO₂ flux variability from an observation-driven ocean mixed-layer scheme, Biogeosciences, 11, 4599–4613, 10.5194/bg-11-4599-2014, 2014.
Roten, D., Lin, J. C., Das, S., and Kort, E. A.: Constraining Sector-Specific CO2 Fluxes Using Space-Based XCO2 Observations Over the Los Angeles Basin, Geophysical Research Letters, 50, e2023GL104376, https://doi.org/10.1029/2023GL104376, 2023.
Sato, H., Itoh, A., and Kohyama, T.: SEIB–DGVM: A new Dynamic Global Vegetation Model using a spatially explicit individual-based approach, Ecological Modelling, 200, 279–307, 2007.
Shukla, P. R., Skea, J., Slade, R., Al Khourdajie, A., van Diemen, R., McCollum, D., Pathak, M., Some, S., Vyas, P., and Fradera, R.: Climate change 2022: Mitigation of climate change, Contribution of working group III to the sixth assessment report of the Intergovernmental Panel on Climate Change, 10, 9781009157926, 2022.
Song, L., Chang, J., and Yi, J.: A Bottom-Up Carbon Emission Assessment Model for Carbon Emission Control at the Level of Rural Detailed Planning, Land, 13, 1023, 2024.
Stagakis, S., Feigenwinter, C., Vogt, R., and Kalberer, M.: A high-resolution monitoring approach of urban CO2 fluxes. Part 1 - bottom-up model development, Science of The Total Environment, 858, 160216, https://doi.org/10.1016/j.scitotenv.2022.160216, 2023.

https://doi.org/10.5194/egusphere-2026-2619
Preprint. Discussion started: 18 June 2026

Stohl, A.: Computation, accuracy and applications of trajectories—A review and bibliography, Atmospheric Environment, 32, 947–966, https://doi.org/10.1016/S1352-2310(97)00457-3, 1998.
Stohl, A., Hittenberger, M., and Wotawa, G.: Validation of the lagrangian particle dispersion model FLEXPART against large-scale tracer experiment data, Atmospheric Environment, 32, 4245–4264, https://doi.org/10.1016/S1352-2310(98)00184-8, 1998.
Stohl, A., Forster, C., Frank, A., Seibert, P., and Wotawa, G.: Technical note: The Lagrangian particle dispersion model FLEXPART version 6.2, Atmos. Chem. Phys., 5, 2461–2474, 10.5194/acp-5-2461-2005, 2005.
Su, W., Wang, B., Chen, H., Zhu, L., Zheng, X., and Chen, S. X.: A new global carbon flux estimation methodology by assimilation of both in situ and satellite CO2 observations, npj Climate and Atmospheric Science, 7, 287, 10.1038/s41612-024-00824-w, 2024.
Tarantola, A.: Inverse problem theory and methods for model parameter estimation, SIAM2005.
Thompson, R. L. and Stohl, A.: FLEXINVERT: an atmospheric Bayesian inversion framework for determining surface fluxes of trace species using an optimized grid, Geosci. Model Dev., 7, 2223–2242, 10.5194/gmd-7-2223-2014, 2014.
Thompson, R. L., Krishnankutty, N., Pisso, I., Schneider, P., Stebel, K., Sasakawa, M., Stohl, A., and Platt, S. M.: Efficient use of a Lagrangian particle dispersion model for atmospheric inversions using satellite observations of column mixing ratios, Atmos. Chem. Phys., 25, 12737–12751, 10.5194/acp-25-12737-2025, 2025.
Thomson, D. J.: Criteria for the selection of stochastic models of particle trajectories in turbulent flows, Journal of Fluid Mechanics, 180, 529–556, 10.1017/S0022112087001940, 1987.
Thornton, P. E., Law, B. E., Gholz, H. L., Clark, K. L., Falge, E., Ellsworth, D. S., Goldstein, A. H., Monson, R. K., Hollinger, D., and Falk, M.: Modeling and measuring the effects of disturbance history and climate on carbon and water budgets in evergreen needleleaf forests, Agricultural and forest meteorology, 113, 185–222, 2002.
Varghese, S., Langmann, B., Ceburnis, D., and O'Dowd, C. D.: Effect of horizontal resolution on meteorology and air-quality prediction with a regional scale model, Atmospheric Research, 101, 574–594, https://doi.org/10.1016/j.atmosres.2011.02.007, 2011.
Wang, W. and Nemani, R.: Dynamic responses of atmospheric carbon dioxide concentration to global temperature changes between 1850 and 2010, Advances in Atmospheric Sciences, 33, 247–258, 10.1007/s00376-015-5090-y, 2015.
Wang, X., Gao, F., Tan, Q., and Xiao, Z.: Planning for ventilation corridor in city with high-frequency static wind: A case study of ChengDu city, City Plan. Rev, 44, 129–136, 2020.
Wu, K., Palmer, P. I., Wu, D., Jouglet, D., Feng, L., and Oda, T.: Theoretical assessment of the ability of the MicroCarb satellite city-scan observing mode to estimate urban CO2 emissions, Atmos. Meas. Tech., 16, 581–602, 10.5194/amt-16-581-2023, 2023.
Xia, X., Jian, L., Ouyang, K., Liu, X., Liang, X., Zhang, Y., and Li, B.: Assessment of Ventilation Potential and Construction of Wind Corridors in Chengdu City Based on Multi-Source Data and Multi-Model Analysis, Land, 13, 1671, 2024.
Xiao, L., Wang, W., Luo, Y., and Liu, X.: Evolutionary Analysis of Synergistic Development of Green and Low-Carbon Industries in Chengdu-Chongqing Region, The Eighteenth International Conference on Management Science and Engineering Management, Singapore, 2024//, 1388–1399,
Xiong, J., Li, J., Gao, F., and Zhang, Y.: City Wind Impact on Air Pollution Control for Urban Planning with Different Time-Scale Considerations: A Case Study in Chengdu, China, Atmosphere, 14, 1068, 2023.
Ye, X., Lauvaux, T., Kort, E. A., Oda, T., Feng, S., Lin, J. C., Yang, E. G., and Wu, D.: Constraining fossil fuel CO2 emissions from urban area using OCO-2 observations of total column CO2, Journal of Geophysical Research: Atmospheres, 125, e2019JD030528, 2020.
Yu, J., Yu, L., Luo, Y., and Zhang, P.: Research on the development path of Chengdu as a low-carbon city under the dual constraints of carbon emission and economic growth, Frontiers in Environmental Science, Volume 12 - 2024, 10.3389/fenvs.2024.1494848, 2024.
Zhang, D., Huggins, J., Li, Q., Ramachandran, S., Serbin, S., Webb, C., Zuo, Z., and Dietze, M.: Mapping the North American Terrestrial Carbon Cycle: A Process-based Reanalysis Using State Data Assimilation (SDA), bioRxiv, 2026.2002.2025.708030, 10.64898/2026.02.25.708030, 2026.
Zhang, L., Jiang, F., Mao, Y., Lv, G., Wang, H., Feng, S., and Ju, W.: A Top-Down Method for Estimating Regional Fossil Fuel Carbon Emissions Based on Satellite XCO2 Retrievals, Remote Sensing, 17, 447, 2025.

https://doi.org/10.5194/egusphere-2026-2619
Preprint. Discussion started: 18 June 2026

Zhao, S., Yang, Y., Ma, L., Bai, Z., Feng, Y., Liu, Q., Wang, Q., Chen, Y., Wang, F., Teng, J., Zhao, L., Xie, Y., Dai, Y., Yu, L., Zhou, Y., and Xiong, Y.: A review of satellite remote sensing for pollution control and carbon reduction in China, International Journal of Applied Earth Observation and Geoinformation, 146, 105109, https://doi.org/10.1016/j.jag.2026.105109, 2026.

Zhao, X., Wu, L., Wang, J., and Mao, H.: Concentration variation and law of greenhouse gases in Xining, IOP Conference Series: Earth and Environmental Science, 233, 042053, 10.1088/1755-1315/233/4/042053, 2019.

Zhou, X., Zhang, C., Li, Y., and Zhang, Z.: Comparison of Spring Wind Gusts in the Eastern Part of the Tibetan Plateau and along the Coast: The Role of Turbulence, Remote Sensing, 15, 3655, 2023.

Yao, X.: FEISSO demonstration dataset for urban CO2 flux inversion in Weifang, China, Zenodo [data set], https://doi.org/10.5281/zenodo.20073187, 2026.